Amino Acid Shortages as Cancer Vulnerabilities

Aminozuur Tekorten als Kwetsbaarheden voor Kanker

Thesis

to obtain the degree of Doctor from the
Erasmus University Rotterdam
by command of the
rector magnificus

Prof.dr. R.C.M.E. Engels

and in accordance with the decision of the Doctorate Board.
The public defence shall be held on

Wednesday, 3rd June, 2020 at 13:30 hrs

by

Jianhui (Jane) Sun

Born in Longkou, China

Erasmus University Rotterdam

Doctoral Committee:

Promotor:

Prof. dr. R. Agami

Other members:

Dr. F.N. Van Leeuwen

Prof. dr. C.R. Berkers

Prof.dr. R. Fodde

Table of Contents

List of Abbreviations

ASNase	L-asparaginase
CRISPR	Clustered Regularly Interspaced Short Palindromic Repeats
SLC1A1	Solute carrier family 1 member 1
SLC1A2	Solute carrier family 1 member 2
SLC1A3	Solute carrier family 1 member 3

SLC1A6	Solute carrier family 1 member 6
SLC1A7	Solute carrier family 1 member 7
SLC25A1	Solute carrier family 25 member 1
ASNS	Asparagine synthetase
EIF2AK4 (GCN2)	Eukaryotic translation initiation factor 2 alpha kinase 4
ATF4	Activating transcription factor 4
TCA cycle	Tricarboxylic acid cycle
ALL	Acute lymphoblastic leukemia
RNA	Ribonucleic acid
sgRNA	Single guide RNA
DNA	Deoxyribonucleic acid
cDNA	Complementary DNA
MAGeCK	Model-based analysis of genome-wide CRISPR-Cas9 knockout
FDR	False discovery rate
TCGA	The Cancer Genome Atlas
KIRC	Kidney renal clear cell carcinoma
KIRP	Kidney renal papillary cell carcinoma
LIHC	Liver hepatocellular carcinoma
STAD	Stomach adenocarcinoma
KO	Knock-out
mRNA	Messenger RNA
UCPH-101	$C_{27}H_{22}N_2O_3$
TFB-TBOA	$C_{19}H_{17}F_3N_2O_6$
LC-MS	Liquid-chromatography mass spectrometry
OAA	Oxaloacetic acid
UMP	Uridine monophosphate
CMP	Cytidine monophosphate
PEP	Phosphoenolpyruvate
NADH	Nicotinamide adenine dinucleotide (reduced form)
NAD^+	Nicotinamide adenine dinucleotide (oxidized form)
NADPH	Nicotinamide adenine dinucleotide phosphate (reduced form)
$NADP^+$	Nicotinamide adenine dinucleotide phosphate (oxidized form)
FAD	Flavin adenine dinucleotide
GSSG	Glutathione disulfide
HMG-CoA	3-hydroxy-3-methylglutaryl-CoA
SREBP	Sterol regulatory element-binding protein
VEGFA	Vascular endothelial growth factor A
LDHA	Lactate dehydrogenase A
BrdU	Bromodeoxyuridine

Chapter 2

SLC1A3 contributes to L-asparaginase resistance in cancer cells

Jianhui Sun[1,2], Remco Nagel[1], Esther A. Zaal[3], Alejandro Piñeiro Ugalde[1], Ruiqi Han[1,2], Natalie Proost[4], Ji-Ying Song[5], Abhijeet Pataskar[1], Artur Burylo[6], Haigen Fu[7], Gerrit J Poelarends[7], Marieke van de Ven[4], Olaf van Tellingen[6], Celia R. Berkers[3,8], Reuven Agami[1,2,*]

[1]Division of Oncogenomics, Oncode institute, The Netherlands Cancer Institute, Plesmanlaan 121, 1066 CX Amsterdam, the Netherlands.
[2]Department of Genetics, Erasmus University Medical Center, Wytemaweg 80, 3015 CN Rotterdam, the Netherlands.
[3]Biomolecular Mass Spectrometry and Proteomics, Bijvoet Center for Biomolecular Research, Utrecht University, Utrecht, the Netherlands.
[4]Preclinical Intervention Unit and Pharmacology Unit of the Mouse Clinic for Cancer and Ageing (MCCA), The Netherlands Cancer Institute, Amsterdam, the Netherlands.
[5]Division of Experimental Animal Pathology, The Netherlands Cancer Institute, Plesmanlaan 121, 1066CX Amsterdam, the Netherlands.
[6]Division of Pharmacology, The Netherlands Cancer Institute, Plesmanlaan 121, 1066 CX Amsterdam, the Netherlands.
[7]Department of Chemical and Pharmaceutical Biology, University of Groningen, Groningen, The Netherlands.
[8]Department of Biochemistry and Cell Biology, Faculty of Veterinary Medicine, Utrecht University, Utrecht, the Netherlands.

Adopted from EMBO J (2019)38: e102147

[*]**Correspondence and requests for materials should be addressed to RA (r.agami@nki.nl). Tel: +31 205122079; E-mail: r.agami@nki.nl**

Synopsis

- Asparaginase is an effective drug for adolescent acute lymphoblastic leukemia treatment, but toxicity and tolerance hampered further usage in patients with solid tumors.
- A genome-wide functional screen identifies SLC1A3 as a novel contributor to asparaginase resistance in cancer cells, in addition to the known ASNS and GCN2.
- While SLC1A3 expression is typically restricted to brain tissues, high expression level is observed in several tumor types.
- Combined SLC1A3 blockade with asparaginase treatment elicits cell cycle arrest and apoptosis in SLC1A3 positive cancer cells.
- Replenishing intracellular aspartate and glutamate levels by SLC1A3 promotes cancer cell proliferation and metastasis, despite asparaginase-induced shortages.

Abstract

L-asparaginase (ASNase) serves as an effective drug for adolescent acute lymphoblastic leukemia. However, many clinical trials indicated severe ASNase toxicity in patients with solid tumors, with resistant mechanisms not well understood. Here, we took a functional genetic approach and identified SLC1A3 as a novel contributor to ASNase resistance in cancer cells. In combination with ASNase, SLC1A3 inhibition caused cell cycle arrest or apoptosis, and myriads of metabolic vulnerabilities in tricarboxylic acid (TCA) cycle, urea cycle, nucleotides biosynthesis, energy production, oxidation homeostasis and lipid biosynthesis. SLC1A3 is an aspartate and glutamate transporter, mainly expressed in brain tissues, but high expression levels were also observed in some tumor types. Here, we demonstrate that ASNase stimulates aspartate and glutamate consumptions, and their refilling through SLC1A3 promotes cancer cell proliferation. Lastly, *in vivo* experiments indicated that SLC1A3 expression promoted tumor development and metastasis while negating the suppressive effects of ASNase by fueling aspartate, glutamate and glutamine metabolisms despite of asparagine shortage. Altogether, our findings identify a novel role for SLC1A3 in ASNase resistance and suggest that restrictive aspartate and glutamate uptake might improve ASNase efficacy with solid tumors.

Introduction

Treating cancer with amino acid deprivation schemes has achieved limited clinical success so far. Only in acute lymphoblastic leukemia (ALL), the incorporation of L-asparaginase (ASNase) has significantly increased the overall survival rates to ~90% (Pui *et al*, 2009; Broome, 1961; Müller & J.Boos, 1998). ALL cells are auxotrophic for asparagine which was deaminated and depleted by the enzyme ASNase, resulting in cell cycle arrest and apoptosis in ALL cells without affecting normal tissues (Kidd, 1953; Broome, 1961; Pui *et al*, 2009; Ueno *et al*, 1997). Notably, ASNase has a dual asparagine and glutamine deaminase activity, however, its glutaminase activity was not required for anticancer effect in asparagine synthetase (ASNS) negative cancer cells (Chan *et al*, 2014). The therapeutic progress of ASNase in ALL had greatly encouraged its further application for solid tumors. However, many clinical trials reported intolerable toxicity in patients (Hays *et al*, 2013; Haskell *et al*, 1969). ASNS expression has been proposed as a marker for clinical prediction of ASNase resistance (Scherf *et al*, 2000), however, treatment of ALL with ASNase is still effective even though ASNS is expressed (Krall *et al*, 2016; Stams, 2003; Vander Heiden & DeBerardinis, 2017). Interestingly, aspartate metabolism was also predicted to contribute to ASNase sensitivity according to a previous study (Chen *et al*, 2011). Overall, with the exception of ASNS, little is known about the specific resistant mechanisms to ASNase, which has hindered the attempts to broaden ASNase's benefits to patients with solid tumors (Hays *et al*, 2013; Kidd, 1953; Haskell *et al*, 1969; Vander Heiden & DeBerardinis, 2017).

Our previous work has found that ASNase treatment of PC3, a prostate cancer cell line, triggered asparagine shortage accompanied by increased asparagine production through upregulation of ASNS, as indicated by ribosomal and transcriptional profiling (Loayza-Puch *et al*, 2016). This pinpointed a feedback loop under asparagine depleted conditions. Yet, PC3 cells remained proliferative despite of asparagine shortage, suggesting the involvement of other mechanisms responsible for ASNase resistance as upregulated ASNS was not sufficient for asparagine replenishment. Therefore, we used a functional genetic screen in PC3 cells to explore potential vulnerabilities in solid cancer cells to ASNase treatment. We identified SLC1A3, an aspartate/glutamate transporter, as a novel contributor in ASNase resistance, as well as tumor initiation and progression in a mice model for breast cancer metastasis.

Results

A Genome-wide CRISPR-Cas9 screen identifies SLC1A3 as a novel contributor to ASNase resistance in PC3 cells

To determine the optimal ASNase concentration required for performing a genome-wide functional screen, we tested a series of ASNase concentrations in PC3 cells. Fig 1A shows that ASNase at a concentration of 0.3~0.5 U/ml moderately inhibited cell proliferation. As this dosage is within the range used for asparagine depletion in some ALL patients according to previous research (Riccardi *et al*, 1981; Avramis & Panosyan, 2005), we performed the screen and *in vitro* validation under this condition. Due to its essential role in asparagine synthesis, ASNS gene was used as a positive control for the screen. As expected, CRISPR-Cas9 knockout (KO) of ASNS sensitized PC3 cells to ASNase treatment but did not affect cell proliferation under mock-treatment (Fig 1B).

Next, we transduced a genome-wide CRISPR-Cas9 library, consisting of 76,441 single guide RNAs (sgRNAs) targeting 19,114 genes, into PC3 cells, which were further divided into mock and ASNase treated conditions (Fig 1C). Following 20 days of culturing, cells were harvested and subjected to deep sequencing of integrated sgRNAs and MAGeCK bioinformatics analysis of individual sgRNA abundance. Intriguingly, in addition to the expected ASNS gene, this analysis proposed 4 additional genes (FDR<0.003, Fig 1D), whose loss-of-function may impair PC3 cell proliferation following ASNase treatment. Follow-up validations using individual CRISPR vector transductions and cell competitive growth assays successfully validated three out of the four additional hits: EIF2AK4 (GCN2, general control nonderepressible 2), SLC1A3 and SLC25A1 (Figs 1D and EV1A), highlighting the reliability of the screen. Notably, EIF2AK4 was also predictable due to its role in regulating general nutrient deprivation responses (Bunpo *et al*, 2009; Ye *et al*, 2010). The other two hits (SLC1A3 and SLC25A1) are both from the solute carrier family (SLC). SLC1A3 functions as a high-affinity aspartate and glutamate transporter, whose loss-of-function triggered a marked reduction in cell survival and proliferation following ASNase treatment (Figs 1E and EV1B). SLC25A1, a mitochondria citrate carrier, whose loss of function also caused inhibitory effects on cell survival and proliferation in the presence of ASNase, but to a more moderate extent when compared with that of SLC1A3 (Fig EV1A). Due to the relatively strong synergistic effect, from now on, we only focused on the role of SLC1A3 in the context of ASNase.

SLC1A3 is mainly expressed in brain tissues (Fig EV1C), critical for the termination of excitatory neurotransmission (Kanai *et al*, 2013). Recent studies have highlighted the importance of SLC1A3-mediated aspartate uptake for cancer cell proliferation under hypoxia and crosstalk between cancer cells and cancer associated fibroblasts in the tumor niche (Garcia-Bermudez *et al*, 2018; Sullivan *et al*, 2018; Tajan *et al*, 2018; Alkan *et al*, 2018; Bertero *et al*, 2019). We also observed elevated SLC1A3 RNA levels in several tumor types from the TCGA database (especially kidney renal clear cell carcinoma (KIRC, $p = 5.5 \times 10^{-30}$), kidney renal papillary cell carcinoma (KIRP, $p = 2.1 \times 10^{-10}$), liver hepatocellular carcinoma (LIHC, $p = 3.2 \times 10^{-10}$) and stomach adenocarcinoma (STAD, $p = 6.1 \times 10^{-5}$)) (Fig EV1D).

To examine the function of SLC1A3, we tested its cellular aspartate/glutamate transporting function using a radioactive labeled amino acid uptake assay as previously described (Loayza-Puch *et al*, 2017). As predicted, SLC1A3 loss-of-function reduced both aspartate and glutamate uptake in PC3 cells (Fig 1F), also leading to decreased endogenous aspartate (~8-fold) and glutamate (~1.5-fold) levels (Fig 1G). Following ASNase treatment in control PC3 cells, we observed strong depletions of both asparagine and glutamine (Fig 1G), in concordance with its known dual functions. This was followed by a significant reduction in endogenous aspartate and glutamate levels (Fig 1G), indicating a stimulated demand for aspartate and glutamate. Consequently, in SLC1A3-KO PC3 cells, aspartate and glutamate levels was further depleted under ASNase treatment (~16-fold for aspartate and ~3-fold for glutamate, Fig 1G). This observation suggests that SLC1A3-mediated aspartate and glutamate import is required for the maintenance of sufficient intracellular aspartate and glutamate pools to survive ASNase treatment. Of note, the endogenous glutamine level was significantly depleted in SLC1A3-KO PC3 cells, but this had no effect on cell proliferation in the absence of ASNase (Figs 1G and 1E). To directly test the functions of aspartate and glutamate in the context of ASNase, we supplemented SLC1A3-KO PC3 cells with cell-permeable forms of aspartate and glutamate (esterified). Fig 1H shows that both esterified aspartate and esterified glutamate, but not esterified leucine, can restore SLC1A3-KO PC3 cell proliferation in the presence of ASNase. Lastly, we examined a possible role of SLC1A3 to ASNase treatment *in vivo*. We subcutaneously implanted control and SLC1A3-KO PC3 cells into Balb/c nude mice (cAnN/Rj) and examined tumor growth in the absence and presence of ASNase. Fig EV1E shows that loss of SLC1A3 in combination of ASNase treatment impeded tumor growth. Altogether, we conclude that SLC1A3 expression negates the impact of ASNase on PC3 cell survival, proliferation and efficient tumor growth.

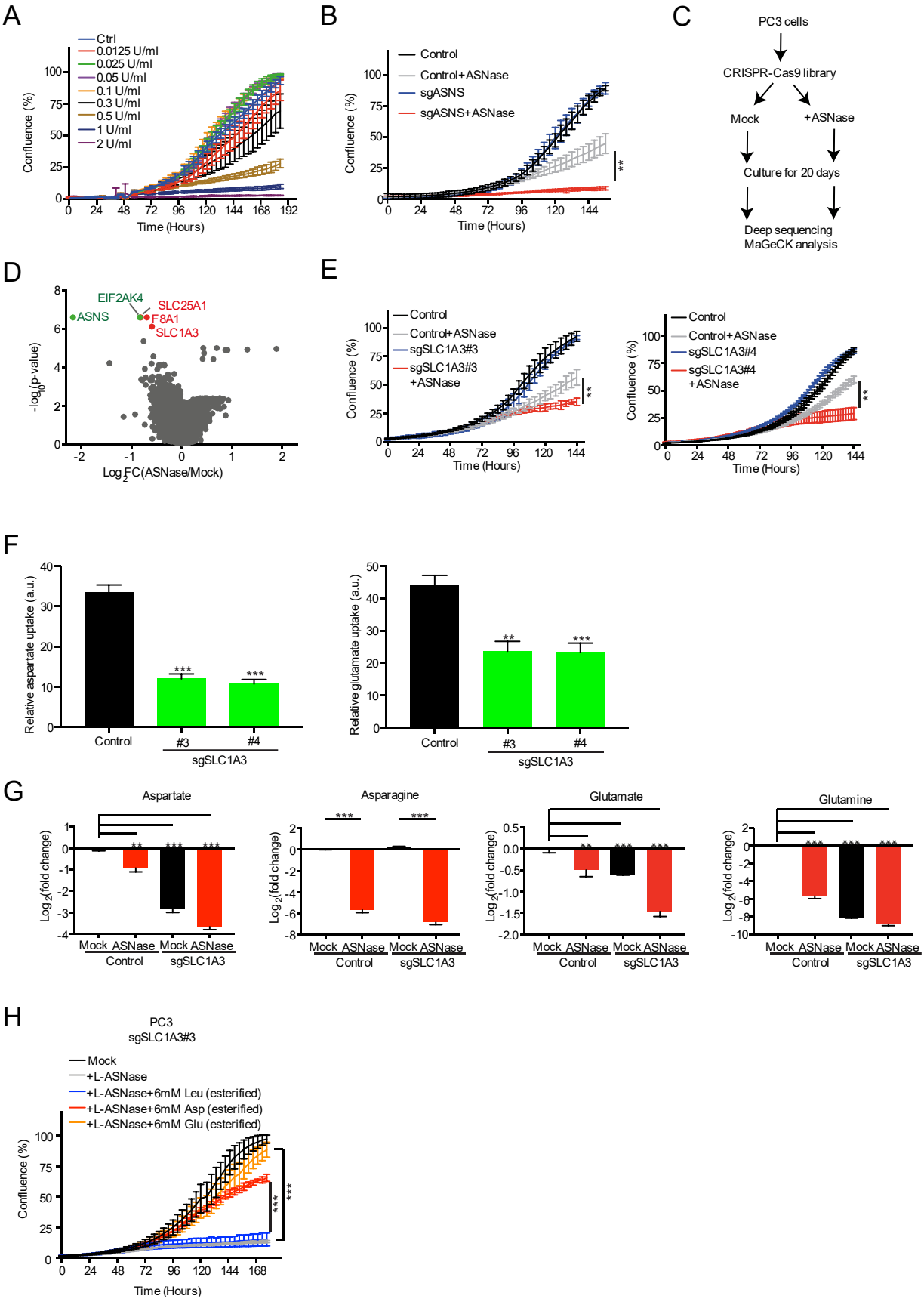
A
Ctrl
0.0125 U/ml
0.025 U/ml
0.05 U/ml
0.1 U/ml
0.3 U/ml
0.5 U/ml
1 U/ml
2 U/ml
Confluence (%)
Time (Hours)
B
Control
Control+ASNase
sgASNS
sgASNS+ASNase
Confluence (%)
Time (Hours)
**
C
PC3 cells
CRISPR-Cas9 library
Mock
+ASNase
Culture for 20 days
Deep sequencing
MaGeCK analysis
D
EIF2AK4
ASNS
SLC25A1
F8A1
SLC1A3
-log10(p-value)
Log2FC(ASNase/Mock)
E
Control
Control+ASNase
sgSLC1A3#3
sgSLC1A3#3
+ASNase
sgSLC1A3#4
sgSLC1A3#4
+ASNase
Confluence (%)
Time (Hours)
F
Relative aspartate uptake (a.u.)
Relative glutamate uptake (a.u.)
Control
#3
#4
sgSLC1A3
G
Aspartate
Asparagine
Glutamate
Glutamine
Log2(fold change)
Mock ASNase
Control
sgSLC1A3
H
PC3
sgSLC1A3#3
Mock
+L-ASNase
+L-ASNase+6mM Leu (esterified)
+L-ASNase+6mM Asp (esterified)
+L-ASNase+6mM Glu (esterified)
Confluence (%)
Time (Hours)

Figure 1. A genome-wide CRISPR-Cas9 screen identifies SLC1A3 as a contributor to L-asparaginase (ASNase) resistance in PC3 cells.

A. IncuCyte cell proliferation curves of PC3 cells treated with the indicated concentrations of ASNase.
B. IncuCyte cell proliferation curves for ASNS knockout (sgASNS) and control (sgNon-targeting) PC3 cells in the absence and presence of ASNase.
C. Flow chart for a genome-wide CRISPR-Cas9 functional screen in PC3 cells.
D. Volcano plots for the MAGeCK pipeline analysis of the sgRNA abundance from the screen. Green dots indicate positive controls and red dots indicate candidates with a fold discovery rate (FDR) <0.003.
E. IncuCyte cell proliferation curves of SLC1A3 knockout (sgSLC1A3) and control (sgNon-targeting) PC3 cells in the absence and presence of ASNase treatment. #3 and #4 represent 2 different sgRNAs targeting SLC1A3.
F. Radioactive labeled aspartate and glutamate uptake measurement in control (sgNon-targeting) and SLC1A3 knockout (sgSLC1A3) PC3 cells. #3 and #4 represent two different sgRNAs targeting SLC1A3. Radioactive labeled leucine uptake was used as a control. Data was normalized to the reads of control PC3 cells.
G. Endogenous levels of aspartate, asparagine, glutamate and glutamine in control (sgNon-targeting) and SLC1A3 knockout (sgSLC1A3) PC3 cells with or without ASNase for 3 days. Median peak intensity was used for the read normalization.
H. IncuCyte cell proliferation curves of SLC1A3 knockout (sgSLC1A3#3) PC3 cells treated with ASNase and supplemented with either esterified-aspartate (6mM) or esterified-glutamate (6mM), and esterified-leucine (6mM) as a control.

Data information:
For IncuCyte proliferation assays, images were taken every 4 hours and the cell confluence was calculated by averaging three mapped images per well. All results were calculated from three replicates and presented as mean ± SD, unless otherwise stated. The *p*-value was calculated by two-tailed unpaired t test by Prism7. ** $p<0.01$, *** $p<0.001$.

SLC1A3 mRNA levels correlate with ASNase sensitivity in different cancer cells

Because SLC1A3 transports both aspartate and glutamate (Figs 1F and 1G), we mainly further used aspartate uptake as a functional readout for SLC1A3. We investigated the correlations between SLC1A3 mRNA level, aspartate uptake and sensitivity to ASNase treatment in a panel of prostate and breast cancer cell lines. As predicted, we observed a general trend where relatively high SLC1A3 mRNA levels indicated high basal aspartate uptake capability (Figs 2A–

B). The exceptions in our cohort were LNCaP, SUM159PT and BT549 cells, with low SLC1A3 mRNA level but high basal aspartate uptake capacity. This can be explained by the relatively high expression of other aspartate/glutamate transporters in these cells (Fig 2C). Accordingly, SLC1A3-KO reduced aspartate uptake level only in SLC1A3-expressing cancer cells (Figs 2A–B). Interestingly, the sensitivity profiles of the tested cancer cell lines to ASNase treatment were generally consistent with the impact of SLC1A3-KO on aspartate uptake, with the exception of BT549 cells (Figs 2B and 2D). To further confirm the correlation between aspartate/glutamate uptake capacity and ASNase sensitivity, we used SLC1A3-deficient MCF7 cells (breast cancer cell line) and DU145 cells (prostate cancer cell line), and established two cancer cell lines overexpressing SLC1A3: MCF7-V5-SLC1A3 and DU145-V5-SLC1A3. Figs 2E–G verified SLC1A3 ectopic expression, its subcellular localization to the plasma membrane, and its capacity to uptake up aspartate in those two cell lines. Importantly, acquired ASNase resistance was observed in both cell lines after the ectopic expression of SLC1A3 (Fig 2H). In line with the above results, the addition of cell-permeable aspartate and glutamate, but not esterified leucine, to DU145 cells, restored cell proliferation under ASNase conditions (Fig 2I). Taken together, we conclude that SLC1A3-mediated aspartate/glutamate uptake promoted ASNase resistance.

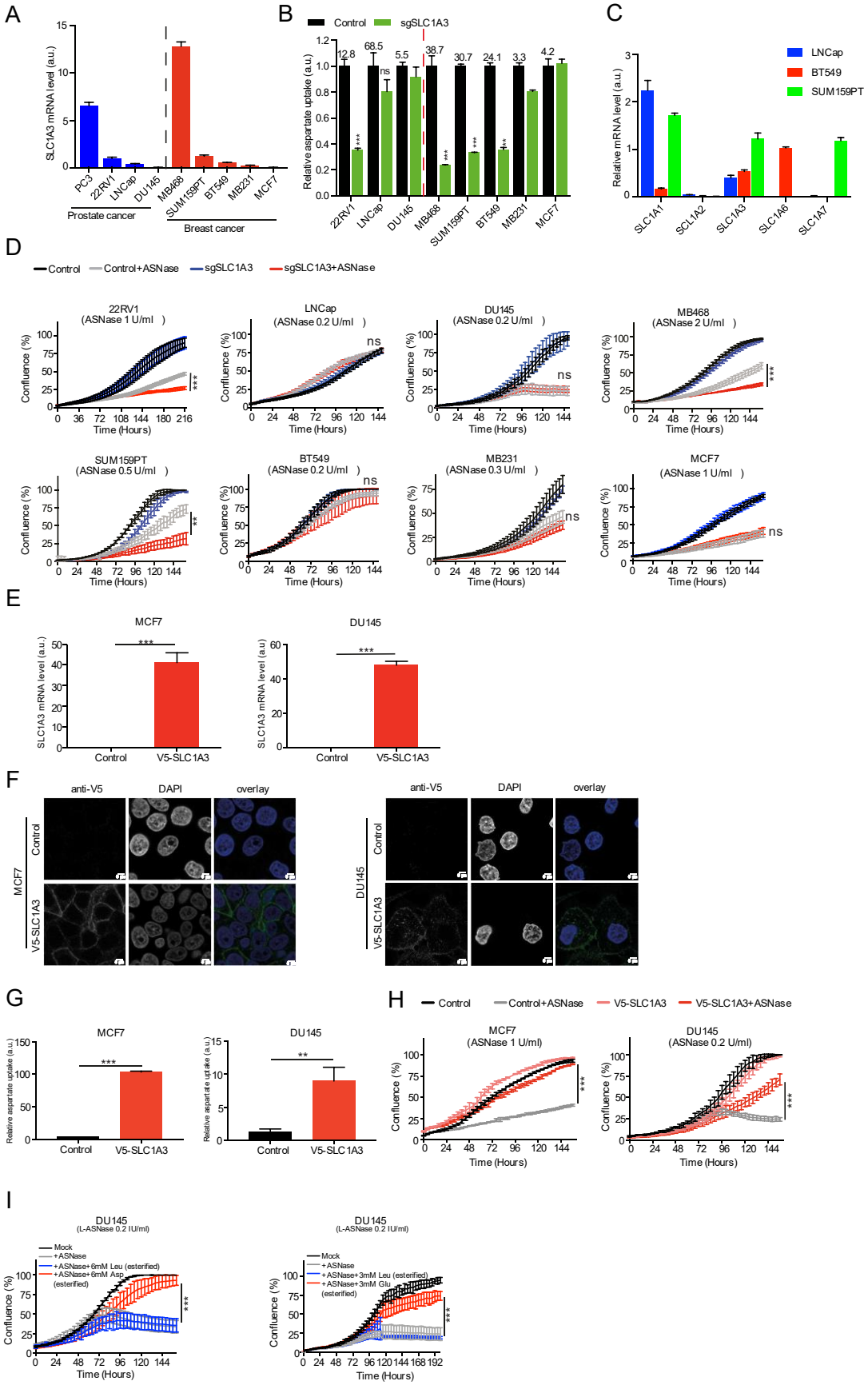
A
SLC1A3 mRNA level (a.u.)
PC3
22RV1
LNCap
DU145
MB468
SUM159PT
BT549
MB231
MCF7
Prostate cancer
Breast cancer
B
Control
sgSLC1A3
Relative aspartate uptake (a.u.)
12.8
68.5
5.5
38.7
30.7
24.1
3.3
4.2
ns
C
LNCap
BT549
SUM159PT
Relative mRNA level (a.u.)
SLC1A1
SCL1A2
SLC1A3
SLC1A6
SLC1A7
D
Control
Control+ASNase
sgSLC1A3
sgSLC1A3+ASNase
22RV1
(ASNase 1 U/ml)
LNCap
(ASNase 0.2 U/ml)
DU145
(ASNase 0.2 U/ml)
MB468
(ASNase 2 U/ml)
SUM159PT
(ASNase 0.5 U/ml)
BT549
(ASNase 0.2 U/ml)
MB231
(ASNase 0.3 U/ml)
MCF7
(ASNase 1 U/ml)
Confluence (%)
Time (Hours)
E
MCF7
DU145
SLC1A3 mRNA level (a.u.)
Control
V5-SLC1A3
F
anti-V5
DAPI
overlay
MCF7
DU145
Control
V5-SLC1A3
G
MCF7
DU145
Relative aspartate uptake (a.u.)
Control
V5-SLC1A3
H
Control
Control+ASNase
V5-SLC1A3
V5-SLC1A3+ASNase
MCF7
(ASNase 1 U/ml)
DU145
(ASNase 0.2 U/ml)
Confluence (%)
Time (Hours)
I
DU145
(L-ASNase 0.2 IU/ml)
Mock
+ASNase
+ASNase+6mM Leu (esterified)
+ASNase+6mM Asp (esterified)
+ASNase+3mM Leu (esterified)
+ASNase+3mM Glu (esterified)
Confluence (%)
Time (Hours)

Figure 2. SLC1A3 expression is linked to ASNase resistance in different cancer cells.

A. RT-qPCR analysis was used to determine the relative SLC1A3 mRNA expression (to GAPDH) in different prostate and breast cancer cell lines, as indicated.
B. The same cell lines (as in panel A) were transduced with either control (sgNon-targeting) or sgSLC1A3. Aspartate uptake levels were determined and compared between control and SLC1A3 KO in these cell lines. Leucine uptake level was used for normalization. The numbers above the control column denote the basal aspartate uptake capacity.
C. RT-qPCR was used to determine the relative mRNA levels (to GAPDH) of aspartate/glutamate transporter genes (SLC1A1, SLC1A2, SLC1A3, SLC1A6 and SLC1A7) in LNCaP, BT549 and SUM159PT cells.
D. The same batch of cancer cells (as in panel B) was subjected to IncuCyte cell proliferation assays in the absence or presence of ASNase at indicated concentrations. 'ns' indicates no significant difference.
E. MCF7 and DU145 cells were transduced with either lentiviral empty vector (control) or lentiviral vector containing a V5-tagged SLC1A3 coding sequence (V5-SLC1A3). Relative SLC1A3 mRNA levels (to GAPDH) were determined by RT-qPCR.
F. Immunofluorescence staining of the V5-tagged SLC1A3 in MCF7 and DU145 cells using anti-V5 antibody. Green staining indicates the plasma membrane localization of V5-SLC1A3 and blue DAPI staining marks the nuclei. Scale bar stands for 5 μm.
G. Relative aspartate uptake levels in control and V5-SLC1A3-expressed MCF7 and DU145 cells. Leucine uptake level was used for normalization.
H. Control and V5-SLC1A3 expressed MCF7 and DU145 cells were subjected to IncuCyte cell proliferation assays with or without ASNase at indicated concentrations.
I. DU145 cells were supplemented with cell-permeable aspartate (6mM, esterified) or glutamate (3mM, esterified) following ASNase treatment, with esterified leucine (6mM or 3mM) as control.

Data information: Results were calculated based on three replicates (except for SUM159 and BT549 in B, n=2) and presented as mean ± SD. The *p*-value was calculated by two-tailed unpaired t test in Prism7. ***p*<0.01, ****p*<0.001. a.u. indicates arbitrary unit.

Combination of SLC1A3 inhibition and ASNase induces metabolic vulnerabilities that impede cancer cell proliferation

Next, we assessed chemical SLC1A3 inhibition in the context of ASNase. We mainly compared two SLC1A3 inhibitors, the selective non-substrate blocker UCPH-101 (Abrahamsen *et al*, 2013) and TFB-TBOA (Shimamoto *et al*, 2004). By aspartate uptake assay, we observed that the inhibitory activity of TFB-TBOA was far more potent than that of UCPH-101, even reaching a

nanomolar level (Fig EV2A). Therefore, we used TFB-TBOA for further experiments. Notably, while TFB-TBOA and ASNase respectively had either no or mild effect on PC3 cell proliferation, their combinational treatment effectively hindered cell proliferation and cell cycle progression (Figs 3A–B and EV2B–D). In addition, TFB-TBOA completely restored the adverse effect of ASNase in DU145-V5-SLC1A3 cells but had no influence on DU145 wildtype cells (Figs 3A and 3C). Interestingly, while the combinational treatment impaired cell cycle progression in PC3 cells, it caused apoptosis in DU145-V5-SLC1A3 cells (Figs 3C and EV2E).

Next, we investigated the effects of combined ASNase and SLC1A3 inhibition on intracellular amino acids and key metabolites levels by liquid-chromatography mass spectrometry (LC-MS). In concordance with SLC1A3-KO, SLC1A3 inhibition by TFB-TBOA promoted further depletions of aspartate and glutamate pools in PC3 cells in the presence of ASNase (Fig 3D). However, in contrast to SLC1A3-KO, TFB-TBOA didn't perturb aspartate, glutamate and glutamine levels, probably due to the short drug exposure time compared with the genetic manipulation. Notably, combined ASNase and SLC1A3 inhibition induced a marked reduction in argininosuccinate from the urea cycle (Fig 3E). This effect can be reasoned by the lack of aspartate availability as a substrate for argininosuccinate synthesis (Rabinovich *et al*, 2015). Moreover, nucleotide synthesis and tricarboxylic acid (TCA) cycle replenishments were also impaired (Fig 3E), probably due to the deficit of aspartate as previously described (Rabinovich *et al*, 2015; Ahn & Metallo, 2015). We also observed that combinational treatment disturbed the NAD^+/NADH homeostasis, an important indicator for cellular energy assessment and oxidative status (Fig 3E). And strong lactate depletion was detected, at least partly due to the depletion of NADH (Fig 3E). Moreover, levels of carnitine metabolites (important transporters for lipid metabolism) was also perturbed under combinational conditions (Fig 3E). Above all, in SLC1A3 expressed PC3 cells, ASNase and TFB-TBOA impact metabolites involved in the urea cycle, nucleotides synthesis, energy production by TCA cycle and glycolysis, as well as oxidative homeostasis and lipid metabolism. These metabolic alterations further explain why PC3 cells resist ASNase treatment but become vulnerable once SLC1A3 is either genetically depleted or chemically blocked.

We also probed the key metabolites in DU145 and DU145-V5-SLC1A3 cells. In DU145 cells (lacking SLC1A3 expression), ASNase alone was sufficient to induce a similar metabolic profile as obtained in PC3 treated with ASNase and SLC1A3 inhibition (Figs EV2F). Ectopic

expression of SLC1A3 negated these adverse effects, and accordingly, the addition of TFB-TBOA restored those perturbations in DU145-V5-SLC1A3 cells (Figs EV2F).

Then we inquired whether ASNase treatment promotes a special usage of cellular aspartate/glutamate. For that purpose, we conducted metabolic flux studies using [$^{13}C_4$,^{15}N] L-aspartate and [$^{13}C_5$,^{15}N] L-glutamate in DU145-V5-SLC1A3 cells. Notably, as observed before (Sullivan *et al*, 2018), exogenous labeled aspartate was barely incorporated to the intracellular asparagine pool. Instead, both labeled aspartate and glutamate were actively used to replenish downstream metabolisms, such as TCA cycle, urea cycle and nucleotide synthesis. However, following ASNase treatment, the relative profiles of labeled metabolites remained generally similar to mock treated cells, except for increased incorporation into glutamine from labeled glutamate (Fig EV3B–C). Thus, ASNase treatment did not induce significant perturbations in the general metabolic usage of aspartate and glutamate in cancer cells.

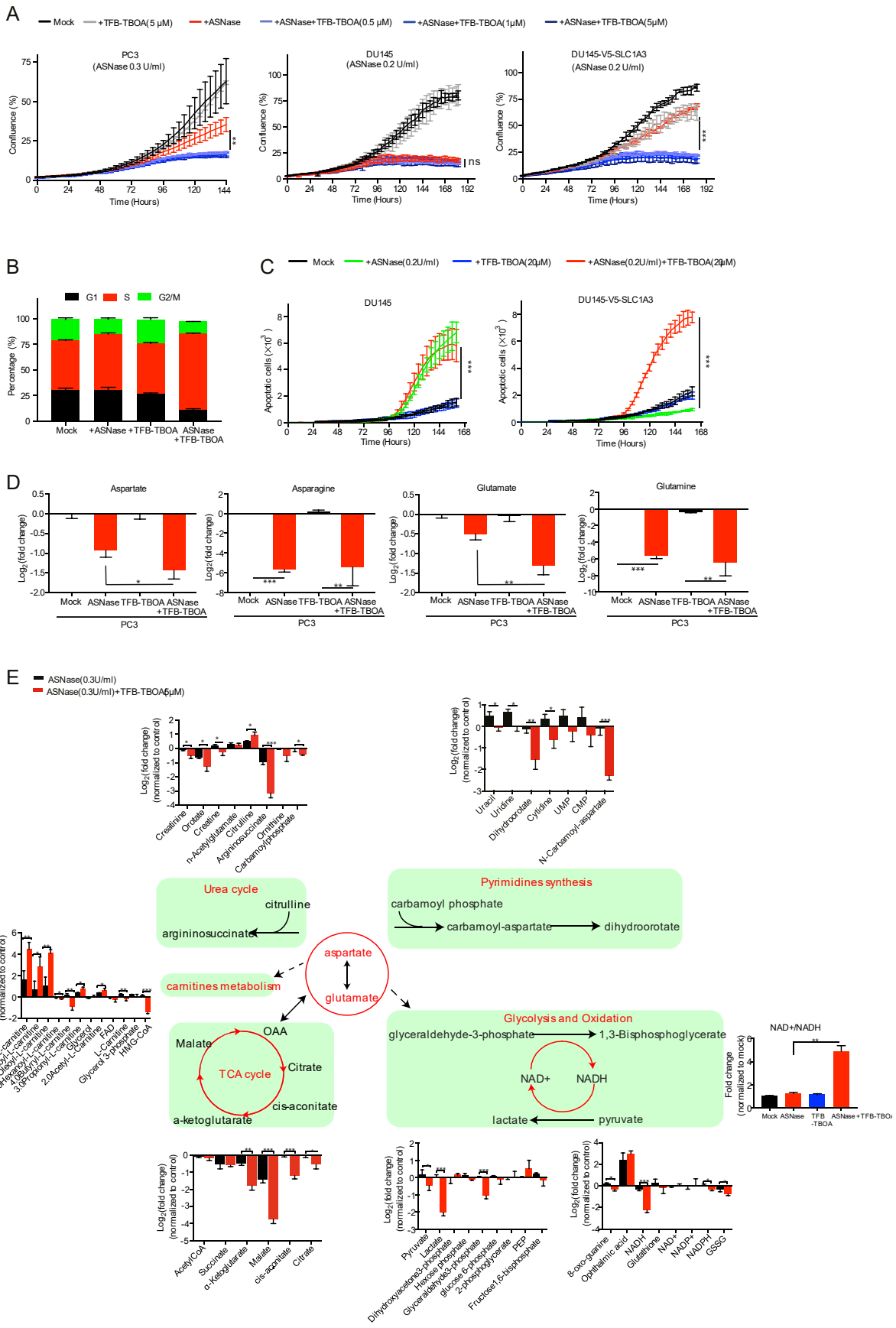
A
Mock
+TFB-TBOA(5 μM)
+ASNase
+ASNase+TFB-TBOA(0.5 μM)
+ASNase+TFB-TBOA(1μM)
+ASNase+TFB-TBOA(5μM)
PC3
(ASNase 0.3 U/ml)
DU145
(ASNase 0.2 U/ml)
DU145-V5-SLC1A3
(ASNase 0.2 U/ml)
Confluence (%)
Time (Hours)
ns
B
G1
S
G2/M
Percentage (%)
Mock
+ASNase
+TFB-TBOA
ASNase +TFB-TBOA
C
Mock
+ASNase(0.2U/ml)
+TFB-TBOA(20μM)
+ASNase(0.2U/ml)+TFB-TBOA(20μM)
DU145
DU145-V5-SLC1A3
Apoptotic cells (×10³)
Time (Hours)
D
Aspartate
Asparagine
Glutamate
Glutamine
Log2 (fold change)
Mock
ASNase
TFB-TBOA
ASNase +TFB-TBOA
PC3
E
ASNase(0.3U/ml)
ASNase(0.3U/ml)+TFB-TBOA(5μM)
Log2(fold change) (normalized to control)
Creatinine
Orotate
Creatine
n-Acetylglutamate
Citrulline
Argininosuccinate
Ornithine
Carbamoylphosphate
Uracil
Uridine
Dihydroorotate
Cytidine
UMP
CMP
N-Carbamoyl-aspartate
Urea cycle
citrulline
argininosuccinate
Pyrimidines synthesis
carbamoyl phosphate
carbamoyl-aspartate
dihydroorotate
aspartate
glutamate
carnitines metabolism
OAA
Malate
TCA cycle
Citrate
cis-aconitate
a-ketoglutarate
Glycolysis and Oxidation
glyceraldehyde-3-phosphate
1,3-Bisphosphoglycerate
NAD+
NADH
lactate
pyruvate
NAD+/NADH
Fold change (normalized to mock)
Mock
ASNase
TFB-TBOA
ASNase +TFB-TBOA
16:0Palmitoyl-L-carnitine
14:0Myristoyl-L-carnitine
18:1Oleoyl-L-carnitine
6:0Hexanoyl-L-carnitine
4:0Butyryl-L-carnitine
3:0Propionyl-L-carnitine
2:0Acetyl-L-carnitine
Glycerol
FAD
L-Carnitine
Glycerol 3-phosphate
HMG-CoA
AcetylCoA
Succinate
α-Ketoglutarate
Malate
cis-aconitate
Citrate
Pyruvate
Lactate
Dihydroxyacetone phosphate
Hexose phosphate
Glyceraldehyde3-phosphate
glucose 6-phosphate
2-phosphoglycerate
PEP
Fructose1,6-bisphosphate
8-oxo-guanine
Ophthalmic acid
NADH
Glutathione
NAD+
NADPH
NADPH
GSSG

Figure 3. Combinational treatment of ASNase and SLC1A3 inhibition induced metabolic vulnerabilities and restrains cancer cell proliferation.

A. PC3, DU145 and V5-SLC1A3-DU145 cells were subjected to ASNase and TFB-TBOA treatment at indicated concentrations and cell proliferation was measured by IncuCyte assay.
B. PC3 cells were treated under indicated conditions for 9 days and subjected to BrdU assays to determine cell cycle distributions. ASNase (0.3 U/ml), TFB-TBOA (5 μM).
C. DU145 and V5-SLC1A3-DU145 cells were treated under indicated conditions with ASNase (0.2 U/ml) or TFB-TBOA (20μM) or both, and subjected to IncuCyte analysis for apoptotic cell counts.
D. PC3 cells were treated under ASNase (0.3 U/ml), or TFB-TBOA (5 μM) conditions for 3 days and cell lysates were extracted and intracellular contents of aspartate, asparagine, glutamate and glutamine were determined by liquid-chromatography mass spectrometry (LC-MS).
E. From the same experiment as in panel D, key metabolites involved in urea cycle, pyrimidine synthesis, TCA cycle, oxidation, glycolysis and carnitines metabolism were determined. The NAD^+/NADH ratio of the indicated conditions was calculated and normalized to control (mean± SEM). Dash line indicates indirect effect. TCA cycle: tricarboxylic acid cycle; OAA: oxaloacetic acid; UMP: uridine monophosphate; CMP: cytidine monophosphate; PEP: phosphoenolpyruvate; NADH: nicotinamide adenine dinucleotide (reduced form); NAD^+: nicotinamide adenine dinucleotide (oxidized form); NADPH: nicotinamide adenine dinucleotide phosphate (reduced form); $NADP^+$: nicotinamide adenine dinucleotide phosphate (oxidized form); FAD: flavin adenine dinucleotide; GSSG: glutathione disulfide; HMG-CoA: 3-hydroxy-3-methylglutaryl-CoA.

Data information: Median peak intensity was used for raw data normalization in (D and E). Results were calculated based on three replicates and presented as mean ± SD (unless otherwise stated). The *p*-value was calculated by two-tailed unpaired t test from Prism7. **p*<0.05, ***p*<0.01, ****p*<0.001.

Gene expression analysis indicates the novel role of SLC1A3 in ASNase resistance

To interrogate the influence on differential gene expression profiles by SLC1A3 and ASNase, we performed transcriptome analysis in three cancer cell lines: PC3 (endogenous expression of SLC1A3), DU145 wildtype (SLC1A3 negative) and DU145-V5-SLC1A3 (ectopic expression of SLC1A3). Consistent with the compromised cell cycle progression in PC3 cells (Figs 3B and EV2B–D), genes related to cell cycle progression were inhibited following ASNase and TFB-TBOA combinational treatment (Fig 4A). ASNase-treated DU145 cells presented upregulated apoptotic signatures, corresponding to the apoptosis phenotype observed in these cells following ASNase treatment (Figs 4B and 3C). Intriguingly, the introduction of SLC1A3 to DU145 cells prevented the emergence of the apoptosis signature, which was restored by the addition of TFB-TBOA (Figs 4C and 3B). The molecular pathways related to lipid metabolism,

for example, the biosynthesis of cholesterol, steroid and mevalonate, and the gene expression related to sterol regulatory element-binding protein (SREBP), have been strongly impaired in all three cancer cell lines when SLC1A3 was either chemically blocked or intrinsically absent following ASNase treatment (Figs 4A–C).

More specifically, we observed increased VEGFA mRNA levels after combinational treatment in PC3 cells (Fig EV4A), in line with previous observations that suggested a negative correlation between VEGFA and aspartate level (Garcia-Bermudez *et al*, 2018). Moreover, the decreased mRNA level of lactate dehydrogenase A (LHDA) can explain the depletion in lactate level measured by metabolites profiling (Fig 3E). Though ASNS mRNA level was strongly upregulated by ASNase and SLC1A3 inhibition in DU145-V5-SLC1A3 cells, still, cell death was induced (Fig EV4C). This indicates that elevated asparagine synthesis by ASNS could be insufficient to convey ASNase resistance, which might also be determined by aspartate/glutamate bioavailability.

Altogether, we conclude that the transcriptomic changes (Figs 4A–C) are in concordance with metabolomic perturbations (Figs 3E and EV2F) and cellular outcomes (Figs 3A–C), indicating a novel role of SLC1A3 in cancer cell survival following ASNase treatment.

A

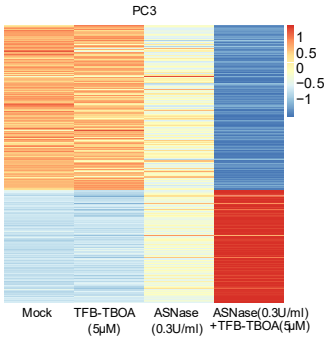
PC3
1
0.5
0
−0.5
−1
Mock
TFB-TBOA (5μM)
ASNase (0.3U/ml)
ASNase(0.3U/ml) +TFB-TBOA(5μM)

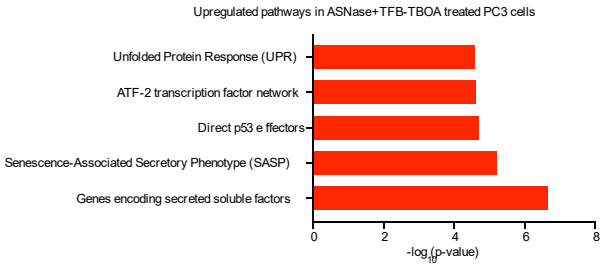
Upregulated pathways in ASNase+TFB-TBOA treated PC3 cells
Unfolded Protein Response (UPR)
ATF-2 transcription factor network
Direct p53 e ffectors
Senescence-Associated Secretory Phenotype (SASP)
Genes encoding secreted soluble factors
0
2
4
6
8
-log10(p-value)

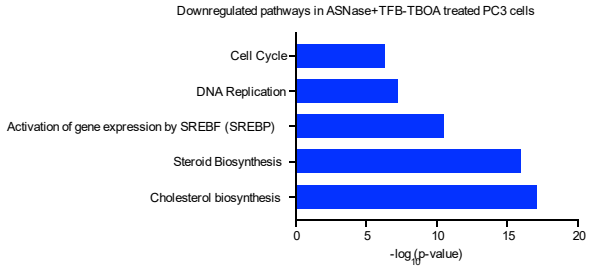
Downregulated pathways in ASNase+TFB-TBOA treated PC3 cells
Cell Cycle
DNA Replication
Activation of gene expression by SREBF (SREBP)
Steroid Biosynthesis
Cholesterol biosynthesis
0
5
10
15
20
-log10(p-value)

B

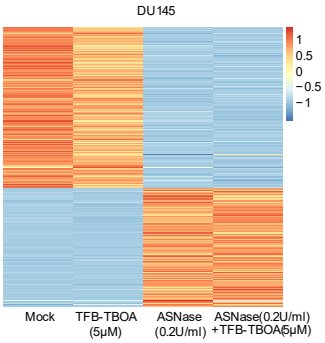
DU145
1
0.5
0
−0.5
−1
Mock
TFB-TBOA (5μM)
ASNase (0.2U/ml)
ASNase(0.2U/ml) +TFB-TBOA(5μM)

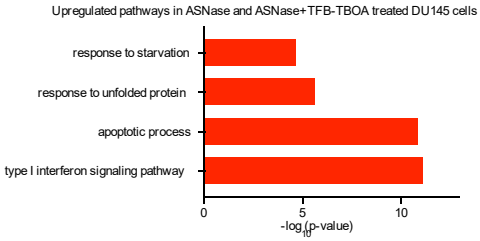
Upregulated pathways in ASNase and ASNase+TFB-TBOA treated DU145 cells
response to starvation
response to unfolded protein
apoptotic process
type I interferon signaling pathway
0
5
10
-log10(p-value)

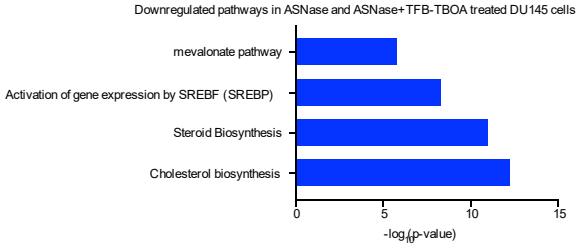
Downregulated pathways in ASNase and ASNase+TFB-TBOA treated DU145 cells
mevalonate pathway
Activation of gene expression by SREBF (SREBP)
Steroid Biosynthesis
Cholesterol biosynthesis
0
5
10
15
-log10(p-value)

C

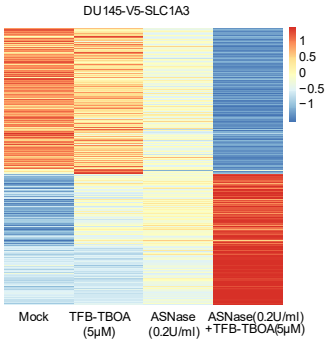
DU145-V5-SLC1A3
1
0.5
0
−0.5
−1
Mock
TFB-TBOA (5μM)
ASNase (0.2U/ml)
ASNase(0.2U/ml) +TFB-TBOA(5μM)

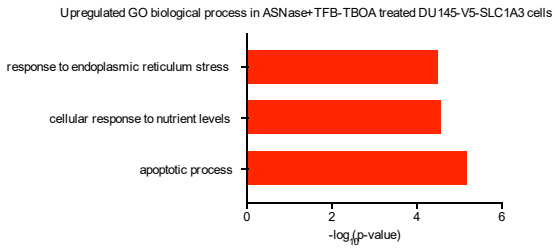
Upregulated GO biological process in ASNase+TFB-TBOA treated DU145-V5-SLC1A3 cells
response to endoplasmic reticulum stress
cellular response to nutrient levels
apoptotic process
0
2
4
6
-log10(p-value)

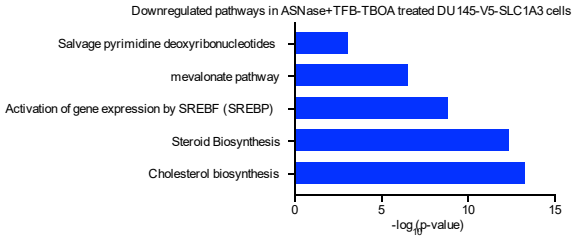
Downregulated pathways in ASNase+TFB-TBOA treated DU145-V5-SLC1A3 cells
Salvage pyrimidine deoxyribonucleotides
mevalonate pathway
Activation of gene expression by SREBF (SREBP)
Steroid Biosynthesis
Cholesterol biosynthesis
0
5
10
15
-log10(p-value)

Figure 4. Gene expression changes pinpoint key pathways involved in SLC1A3-mediated ASNase resistance.

A–C. PC3 (A), DU145 (B) and DU145-V5-SLC1A3 (C) cells were treated with ASNase (0.3 U/ml in A; 0.2 U/ml in B and C), TFB-TBOA (5 μM) for 3 days as indicated and subjected to transcriptome analysis. Bioinformatics pathway or gene ontology (GO) biological process analysis was performed on the sets of genes that were upregulated or downregulated when PC3 cells were treated with ASNase and TFB-TBOA compared to mock. Transcriptome analysis was based on one biological replicate for each cell line and validated by real-time PCR experiments in Figures EV4A–C. Heatmap presents row scaled normalized read counts and the biological signaling pathway enrichment analysis was performed by ToppGene online program (Chen *et al*, 2009).

SLC1A3 expression promotes tumor progression and ASNase resistance in a mouse model for breast cancer metastasis

Next, we set up experiments to examine the role of SLC1A3 in tumor response to ASNase treatment *in vivo*. As a first step, we interrogated the impact of ASNase treatment on asparagine and glutamine levels in mice with human breast cancer xenografts. We orthotopically injected human breast cancer cells (SUM159PT) to mammary fat pads of NOD-Scid IL2Rg-null (NSG) mice, allowed tumors to develop to ~250 mm^3 and then systemically injected 60U ASNase per day for 5 consecutive days. Remarkably, we detected very strong ASNase-induced depletions of asparagine not only in the blood, but also in the mammary fat pad tissues and even within the growing tumors (Fig 5A). However, unlike the glutaminase effect of ASNase *in vitro*, here we detected very modest perturbation in glutamine levels (Fig EV5A). This is probably due to the instant glutamine replenishment under *in vivo* conditions. ASNase treatment could potentially disturb tumor growing environment, at least in the perspective of asparagine.

Next, we employed 4T1, a highly malignant mouse breast cancer cell line, for the assessment of the influence of SLC1A3 on ASNase efficacy *in vivo*. This cell line does not express SLC1A3 (www.biogps.org), does not take up aspartate, and accordingly shows high sensitivity to ASNase treatment (Fig EV5B). As expected, ectopic expression of SLC1A3 (4T1-V5-SLC1A3) promoted exogenous aspartate uptake and restored 4T1 proliferation in the presence of ASNase *in vitro* (Fig EV5B). We therefore implanted 4T1 and 4T1-V5-SLC1A3 cells into the mammary fat pad of either mock or ASNase pretreated NSG mice and measured tumor development. Intriguingly, while the growth of tumors derived from parental 4T1 cells was impaired by ASNase at an early stage (day 9 and 12), SLC1A3-expressing tumors showed no significant differences between ASNase- and mock-treatment (Figs 5B and EV5C). Moreover,

consistent with recent reports (Sullivan *et al*, 2018; Garcia-Bermudez *et al*, 2018), implantation of SLC1A3-expressing 4T1 cells resulted in relatively faster tumor growth compared to that of parental 4T1 cells (Fig EV5D). Once tumors reached the volume of ~500mm^3, mastectomy was performed to remove the primary tumors. The amino acids analysis of the harvested tumor samples by mass spectrometry revealed almost complete depletion of asparagine by ASNase, regardless of SLC1A3 expression status, and slightly reduced aspartate levels in parental 4T1 cells derived tumors following ASNase treatment (Fig 5C). Intriguingly, we also observed depleted glutamine and glutamate levels in control tumors (Fig 5C). This might relate to the absence of SLC1A3 or other aspartate/glutamate transporters in 4T1 cells, which might decelerate glutamine replenishment in the presence of ASNase, at least in this model. Of note, the introduction of SLC1A3 into 4T1 cells (4T1-V5-SLC1A3) increased intratumor aspartate and glutamate levels, and further negated aspartate and glutamine depletions by ASNase treatment at the cost of glutamate consumption (Fig 5C).

Following mastectomy, mice survival rate was scored. In agreement with the effect of ASNase on primary tumor establishment, mice bearing tumors derived from parental 4T1 cells survived better early after ASNase treatment than mock treated mice (Fig EV5E, left). In contrast, ASNase treatment had no effect on the survival rate of mice with SLC1A3-expressing tumors, even at early stage (Fig EV5E, right).

Recently, the bioavailability of asparagine was reported to govern breast cancer metastasis, and ASNase could reduce breast cancer metastasis (Knott *et al*, 2018). From our results above, SLC1A3 mediated aspartate/glutamate imports could affect ASNase treatment. Therefore, we next assessed whether SLC1A3 expression could negate the inhibitory effect of ASNase on cancer cell invasion in a mouse metastasis model for human breast cancer cells as described recently (Knott *et al*, 2018). For this purpose, we used MDA-MB-231 human breast cancer cells whose metastasis burden was reduced by ASNase (Knott *et al*, 2018). Similar to 4T1 cells, MDA-MB-231 cells hardly expressed SLC1A3 (Fig 2A), did not take up aspartate and were highly sensitive to ASNase (Fig EV5F). Consistent with above results (Figs 2G–H), SLC1A3 expression increased aspartate uptake and promoted MDA-MB-231 cell proliferation in the presence of ASNase (Fig EV5F). We therefore introduced MDA-MB-231 and MDA-MB-231-V5-SLC1A3 cells intravenously into NSG mice and assessed the invasive burdens in lung and liver. As previously reported (Knott *et al*, 2018), ASNase treatment reduced metastasis of parental MDA-MB-231 cells to the lung (Fig 5D). In contrast, the introduction of SLC1A3 increased

metastatic burdens and overcame the inhibitory effect by ASNase (Fig 5D). Thus, we conclude that SLC1A3 expression induces tumor progression and ASNase resistance.

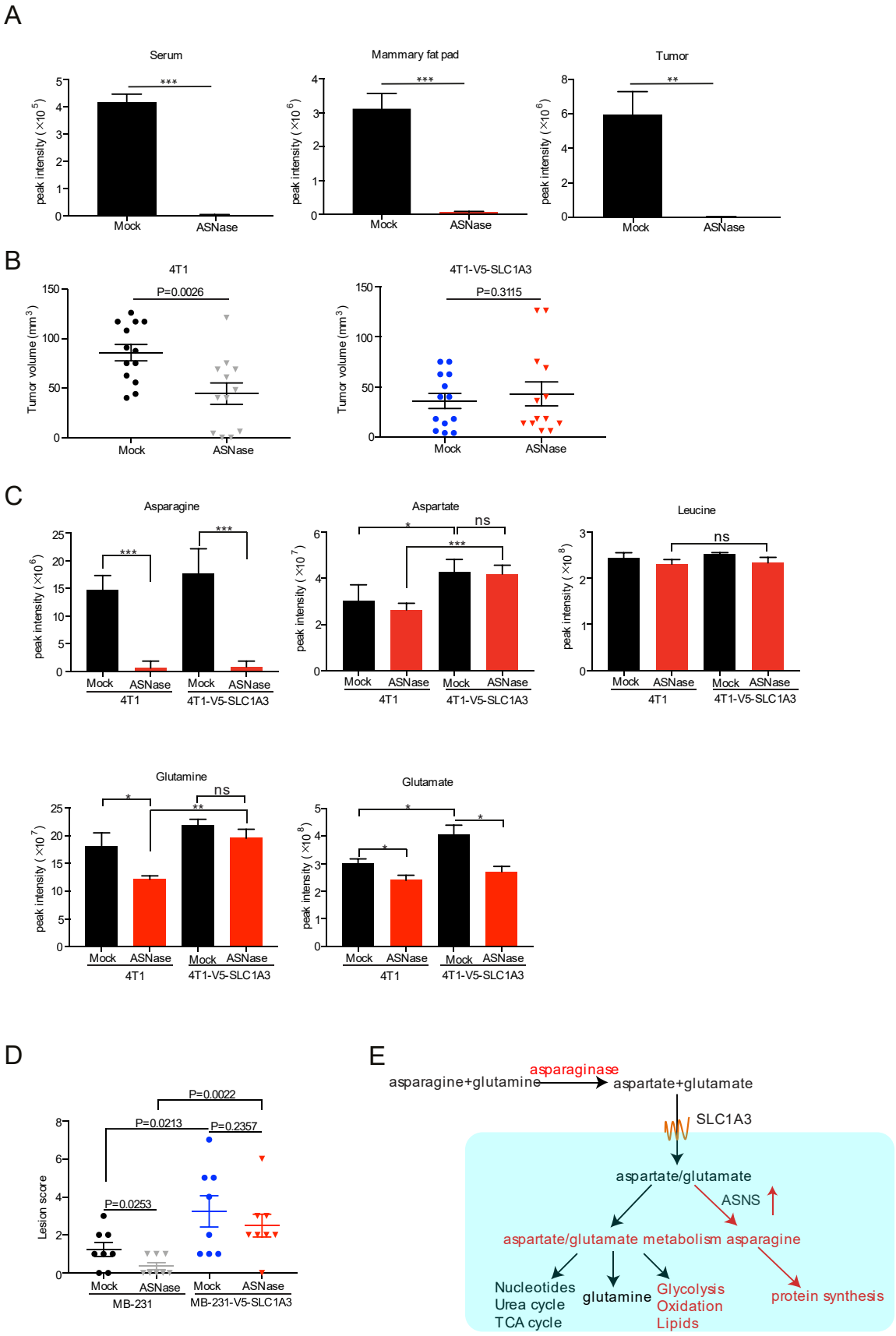
A
Serum
Mammary fat pad
Tumor
peak intensity (×10^5)
peak intensity (×10^6)
***
**
Mock
ASNase
B
4T1
4T1-V5-SLC1A3
P=0.0026
P=0.3115
Tumor volume (mm^3)
C
Asparagine
Aspartate
Leucine
Glutamine
Glutamate
peak intensity (×10^6)
peak intensity (×10^7)
peak intensity (×10^8)
ns
4T1
4T1-V5-SLC1A3
D
Lesion score
P=0.0022
P=0.0213
P=0.2357
P=0.0253
MB-231
MB-231-V5-SLC1A3
E
asparaginase
asparagine+glutamine
aspartate+glutamate
SLC1A3
aspartate/glutamate
ASNS
aspartate/glutamate metabolism asparagine
Nucleotides
Urea cycle
TCA cycle
glutamine
Glycolysis
Oxidation
Lipids
protein synthesis

Figure 5. SLC1A3 expression promotes ASNase resistance and tumor progression in a mice model for breast cancer metastasis.

A. SUM159PT human breast cancer cells were orthotopically injected into the mammary glands of NSG mice. Once SUM159PT tumors reached 250mm^3 volume, mice were treated with mock or ASNase (60U per day) for 5 consecutive days (n=3). Following treatment, mice were sacrificed, and blood, mammary glands and tumors were collected and subjected to mass spectrometry to determine the asparagine level. Essential amino acids were used for the raw data normalization. Data are presented as mean ± SD.
B. The mouse breast cancer cell lines 4T1 and 4T1-V5-SLC1A3 were orthotopically implanted into the mammary glands of pretreated NSG mice. Presented is the volume measurements of arising tumors at day 9. (n=13 mice for each group, except for 4T1+ASNase, n=12). Data are presented as mean ± SEM.
C. From the same experiment in panel B, tumors were surgically removed once reached a volume of ~500mm^3 and collected and subjected to LC-MS to determine the levels of asparagine, aspartate, glutamine and glutamate. Leucine level was used as a control. Results are based on five tumor samples and presented as mean ± SEM.
D. The human breast cancer cell lines MDA-MB-231 and MDA-MB-231-V5-SLC1A3 cells were intravenously injected into pretreated NSG mice. Once mice showed breathing problems, they were sacrificed, and lung and liver were collected and blindly scored for metastasis lesions. The *p*-value was calculated by one-tailed unpaired t test in Prism7. Data are presented as mean ± SEM (n=8).
E. A schematic model depicting how SLC1A3-mediated aspartate and glutamate uptake promotes ASNase resistance.

Data information: The pretreatment started 2 days before the injection of cancer cells. And mice were either injected with 60 U ASNase or saline per day. The *p*-value was calculated by two-tailed unpaired t test in Prism7, unless otherwise stated. *p<0.05, **p<0.01, ***p<0.001.

Discussion

Although asparagine deprivation by ASNase was discovered as an effective treatment in lymphomas approximately 5 decades ago, its clinical implementation to other tumor types failed (Clarkson *et al*, 1970; Pui *et al*, 2009; Hays *et al*, 2013). The resistant mechanism to ASNase treatment in solid tumors was mainly attributed to the activation of the general amino acid sensing machinery (GCN2) and asparagine synthesis by ASNS via the GCN2-ATF4-ASNS axis (Scherf *et al*, 2000; Ye *et al*, 2010; Bunpo *et al*, 2009; Nakamura *et al*, 2018). However, the expression of ASNS in ALL didn't compromise ASNase effectivity (Vander Heiden & DeBerardinis, 2017), indicating that the ubiquitous activation of the GCN2-ATF4-ASNS axis in response to nutrient deprivation might be essential, but not sufficient to induce ASNase resistance. Very recently, protein degradation was proposed to contribute to ASNase resistance in ALL (Hinze *et al*, 2019), however, its contribution in the context of solid tumors is not known yet. Here, we described the identification of SLC1A3, an aspartate/glutamate transporter, as a novel contributor to ASNase resistance and metastasis in cancer cells. As SLC1A3 is specifically expressed in brain tissues, this expression pattern may be beneficial to guide ASNase treatment in solid tumors.

ASNase could break down both asparagine and glutamine, even though its glutaminase activity was not required for ASNS-negative cancer cells (Chan *et al*, 2014). Moreover, ASNase was found effective in treating solid tumors with intrinsic loss of ASNS (Li *et al*, 2019). We observed that in cell culture conditions, both asparagine and glutamine were robustly depleted by ASNase (Fig 1G). However, *in vivo* conditions, asparagine was far more effectively depleted than glutamine (Figs 5C and EV5A), probably due to the abundant bioavailability and timely replenishment of glutamine that reduced the effect of glutaminase activity of ASNase. The importance of asparagine to tumor cell survival was further highlighted in recent studies. Ye at al., has demonstrated the importance of asparagine synthesis via GCN2-ATF4 axis for tumor cell survival during nutrient deprivation (Ye *et al*, 2010). And it has been demonstrated the essential role of asparagine in promoting cancer cell proliferation and breast cancer metastasis (Krall *et al*, 2016; Pavlova *et al*, 2018; Knott *et al*, 2018). Altogether, our study provides another support for the role of asparagine in cancer biology, and puts forward the potential usage of ASNase in cancer therapy.

According to a previous study, aspartate metabolism was predicted to contribute to ASNase resistance in primary ALL samples (Chen *et al*, 2011). Our results that ASNase resistance could be provoked by either ectopic SLC1A3 expression or the supplementation of membrane permeable aspartate/glutamate strongly support this hypothesis (Figs 1H and 2H–I). It indicates that SLC1A3-mediated fueling of endogenous aspartate/glutamate levels is a novel contributor to ASNase resistance. Moreover, aspartate was the second most enriched amino acid (after asparagine) for genes related to epithelial-to-mesenchymal transition (Knott *et al*, 2018). In line with this, we observed that SLC1A3 expression could promote cancer cell metastasis, regardless of asparagine bioavailability (Figs 5D and EV5E). Even though recent studies mainly focused on SLC1A3-mediated aspartate uptake (Alkan *et al*, 2018; Garcia-Bermudez *et al*, 2018; Sullivan *et al*, 2018; Tajan *et al*, 2018), we could not exclude the role of glutamate, which could be converted to aspartate via oxidative or reductive carboxylation. This is supported by our findings that both aspartate and glutamate could rescue ASNase toxicity in SLC1A3 KO or negative cancer cells (Figs 1H and 2I).

Notably, we demonstrate that SLC1A3 inhibition in combination with ASNase treatment could hinder cancer cell proliferation by inducing either cell cycle arrest or apoptosis, which was observed in ALL cells following ASNase treatment (Kidd, 1953; Broome, 1961; Pui *et al*, 2009; Ueno *et al*, 1997). Metabolic and transcriptomic profiles of cells treated with ASNase and SLC1A3 inhibition indicated numerous defects in many critical processes (Figs 3E and EV2F). Intriguingly, in addition to the well-known engagements in urea cycle, nucleotide synthesis and TCA cycle replenishments (Van Vranken & Rutter, 2015; Rabinovich *et al*, 2015; Sullivan *et al*, 2015), aspartate and glutamate metabolisms might also directly or indirectly influence energy production, oxidation homeostasis and lipid metabolism following ASNase treatment (Fig 5E).

Our metabolomic and “diricore” analyses indicated that ASNase-treated SLC1A3-expressing cancer cells and tumors still present asparagine shortage (Figs 5A and 5C) (Loayza-Puch *et al*, 2016). Consistent with a previous study (Sullivan *et al*, 2018), our metabolic flux assays demonstrated that asparagine pool was not efficiently replenished by labeled aspartate (Fig EV3A). In mammalian cells, the lack of asparaginase activity prohibits asparagine utilization for the production of other amino acids or for the biosynthesis of metabolic intermediates (Pavlova *et al*, 2018). Thus, intracellular asparagine seems to be mostly consumed for protein synthesis, and the cells seem to be dependent on exogenous asparagine.

Homologues of SLC1A3 (SLC1A1, SLC1A2, SLC1A6 and SLC1A7) can also transport aspartate/glutamate (Kanai *et al*, 2013). It remains to be further investigated whether these transporters also contribute to ASNase resistance in some cancer cells. The compound TFB-TBOA could potently inhibited SLC1A3, which leads to the negation of SLC1A3 in ASNase resistance *in vitro*. However, *in vivo* tests with TFB-TBOA showed poor pharmacokinetics activity (a sharp drop in serum levels 7 hours post injection, data not shown). Future pharmacological manipulation of TFB-TBA might be needed to improve its *in vivo* performance.

Altogether, using a genome-wide functional genetic approach, we identified SLC1A3, an aspartate/glutamate transporter, as a key determinant in the survival of cancer cells during ASNase treatment. We pinpointed the role of aspartate/glutamate in fueling metabolic pathways related to urea cycle, nucleotide, energy production, oxidation homeostasis, lipid metabolism, and glutamine biosynthesis, in this process. Our results show that solid tumors are amendable to systemic administration of ASNase, opening the possibility of expanding ASNase benefit to solid tumors.

Materials and Methods:

Cell culture

The human prostate cancer cell lines (PC3, DU145, LNCaP and 22RV1) were bought from ATCC and cultured in RPMI (Thermo Fisher Scientific). The human breast cancer cell lines (MCF7, MDA-MB-231 and MDA-MB-468) were cultured in high glucose DMEM. SUM159PT cells (archived in the lab) were cultured in DMEM/F12 1:1 medium with addition of insulin (sigma, I1882-100MG, final concentration of 5 μg/ml) and hydrocortisone (sigma, final concentration of 1 μg/ml). BT549 cells (archived in the lab) were cultured in RPMI with insulin (final concentration of 5 μg/ml). The mouse breast cancer cell line 4T1 was a gift from O. v. Tellingen (Amsterdam, the Netherlands), and cultured in DMEM (high glucose). HEK-293T packaging cell line for lentivirus production were cultured in high glucose DMEM. All the mediums were supplemented with 10% FBS, 1% penicillin/streptomycin except for SUM159PT cells (5% FBS + 1% penicillin/streptomycin). All the cells were cultured in a humidified 37°C incubator with 5% CO_2 injection.

IncuCyte cell proliferation assay

Cells were seeded in 96-well plate (Greiner, 655090) and 3 images per well were taken every 4 hours by the IncuCyte imaging system (Essen Bioscience). Cell confluence per well was calculated by averaging the mapped areas for those 3 images. Experiments were performed with independent triplicates.

Generation of SLC1A3 expression plasmid

SLC1A3 cDNA was amplified from the pLX304-SLC1A3 plasmid kindly gifted by Roderick Beijersbergen (Amsterdam, the Netherlands) using the following primer sequences:

5’-ACAGCGTCTAGACCGGTTAGCGCTAGCTCATTAC-3’ and

5’-CGACAGTTAGCCAGAGAGCTCGCGGCCGCCGCTGT-3’. The resulting product was digested using XbaI (Roche) and NotI (Thermo Fisher Scientific) restriction enzymes and ligated into a pLenti backbone (Korkmaz *et al*, 2016) with compatible sticky ends.

Lentivirus production and infection

A third-generation lentivirus packaging system consisting of pCMV-VSV-G (Addgene#8454), pRSV-Rev (Addgene #12253) and pMDLg/pRRE (Addgene #12252) was co-transfected with lentiCRISPR v2 (addgene: #52961) containing sgRNA. Transfection was performed in HEK-293T cells using PEI (polyethylenimine, Polysciences) and medium was refreshed after 18

hours. Virus was harvested 48 hours after transfection by snap-frozen and stored at -80°C. Target cells were incubated with virus for 24 hours and then medium was refreshed. 36 hours after virus infection, target cells were selected with either puromycin (1 μg/ml) or blasticidine (5 μg/ml) according to the need of the experiments. The selection stopped when no surviving cells remained in the no-transduction control plate and cells were switched to normal culture medium.

CRISPR-Cas9 genome-wide screen in PC3 cells and MAGeCK analysis

PC3 cells were transduced with lentivirus pools containing sgRNAs of a genome-wide CRISPR-Cas9 Brunello library (Doench *et al*, 2016) (addgene #73179) at a multiplicity of infection (moi) of ~ 0.3 and ~1000× representations for each guide. After 2~3 days' recovery from puromycin (1 μg/ml) selection, cells were split into two different conditions: one was subjected to ASNase treatment (0.3 U/ml, ITK) for 20 days, and the other to mock treatment. Two independently replicates were included. Subsequently, genomic DNA was isolated using the phenol-chloroform extraction protocol and sgRNAs were amplified using a two-step PCR protocol for next-generation sequencing. Libraries were sequenced in an Illumina HiSeq-2500 sequencer and raw reads were demultiplexed and analyzed using the in-house perl script XCALIBR (https://github.com/NKI-GCF/xcalibr). The individual sgRNAs abundance were further analyzed using MAGeCK (Li *et al*, 2014) pipeline to find genes statistically depleted during the screening. The MAGeCK software was ran with default options and the 1000 non-targeting sgRNAs included in the CRISPR-Cas9 library were used for control normalization.

Fist PCR forward primer: 5'- ACA CTC TTT CCC TAC ACG ACG CTC TTC CGA TCT NNN NNN GGC TTT ATA TAT CTT GTG GAA AGG ACG -3' and first PCR reverse primer: 5'- GTG ACT GGA GTT CAG ACG TGT GCT CTT CCG ATC TAC TGA CGG GCA CCG GAG CCA ATT CC -3'. The forward primer contained a barcode (NNNNNN) that enabled multiplexing.
Second PCR forward primer: 5'- AAT GAT ACG GCG ACC ACC GAG ATC TAC ACT CTT TCC CTA CAC GAC GCT CTT CCG ATC T -3' and reverse primer: 5'- CAA GCA GAA GAC GGC ATA CGA GAT CGA TGT GTG ACT GGA GTT CAG ACG TGT GCT CTT CCG ATC T -3'.

Competitive cell proliferation assay

PC3 parental cells were stably transfected with pLKO-H_2B-GFP and mixed with plentiv2-sgRNA transfected PC3 cells (GFP-negative) at a ratio of ~3:7 and seeded into 12-well plates in the absence or presence of ASNase (0.3 U/ml). Cells were split every 3~5 days and the ratio of GFP-negative cells among the mixed population was measured by flow cytometry (Calibur, BD

Biosciences). GFP-negative cell counts at each timepoint were normalized to day 0 when the cells were initially mixed.

Radioactive aspartate uptake assay

Cells were counted and seeded one day before the assay in 12-well plates as described (Loayza-Puch *et al*, 2017). After washed twice with PBS, cells were incubated respectively with [^{3}H] L-leucine (in sodium-free uptake buffer) and [^{3}H] L-aspartate (in PBS) for 5 minutes. Next, cells were washed twice with ice-cold PBS and collected with 0.1 M NaOH. The counts for radioactivity was measured by a liquid scintillation analyzer on LSC2910 PerkinElmer Counter. Leucine uptake was used for normalization.

BrdU labeling

For PC3 cells, a final concentration of 10 μM bromodeoxyuridine (BrdU, Sigma) was added to the medium and incubated for 25 mins. Cells were harvested and fixed with 70% cold ethanol at 4°C for 30 minutes. RNase A treatment (final concentration at 0.5 mg/mL) at 37°C for 30 mins was applied. Cells were resuspended in freshly prepared HCl/0.5% Triton solution (for DNA denature) at room temperature for 20 minutes and then neutralized by 0.1 M $Na_2B_4O_7$. After washed once with PBS/Tween, cells were incubated with 1:40 diluted anti-BrdU antibody (Dako) at RT for 30 mins. Cells were incubated with FITC-conjugated anti-mouse Alexa Fluor 488 secondary antibody (1:500, Dako) at RT for 30 mins in the dark. After washing another 2X, cells were then resuspended in PI (20 μg/mL) solution and ready for FACS assay (at least 10,000 cells were gated for each condition).

Metabolite profiling and isotope tracing

1.5×10^5 cells were seeded in 6-well plates and treated for 72 hours as indicated. After washed twice with cold PBS, cells were subjected to 1 ml lysis buffer composed of methanol/acetonitrile/H_2O (2:2:1) for metabolites extractions. The lysates were collected and centrifuged at 16, 000 *g* (4°C) for 15 minutes and the supernatant was transferred to a new tube for further liquid-chromatography mass spectrometry (LC-MS) analysis. The LC-MS analysis procedure and parameters were used as described before (Loayza-Puch *et al*, 2017). Metabolites were identified and quantified using LCquan software (Thermo Scientific) on the basis of exact mass within 5 ppm and further validated by concordance with retention times of standards. Peak intensities were normalized based on median peak intensity of total metabolites or on essential amino acids. For Fig 5A, 10 μl of serum was diluted in 1 ml lysis buffer. For Figs 5A and 5C, 50~100 mg mammary fat pad tissues and tumors were ground in a

mortar under liquid nitrogen, metabolites were extracted by adding 500 μl lysis buffer and sonicated for 10 mins before centrifugation.

For isotope tracing experiment, 2.5×10^5 DU145-V5-SLC1A3 cells were seeded in 6-well plates. Next day, cells were exposed to either mock or ASNase (0.2 U/ml) for 48 hours, and then supplemented with either 1.5 mM [$^{13}C_4$,^{15}N] L-aspartate (Cambridge Isotope Laboratories, CNLM-544-H) and 1.5 mM unlabeled glutamate (Sigma, G8415) or 1.5 mM [$^{13}C_5$,^{15}N] L-glutamate (Cambridge Isotope Laboratories, CNLM-544-H) and 1.5 mM unlabeled aspartate (Bioconnect 47203.01) for 8 hours. Then the cells and the medium were harvested for further analysis as described above.

Total RNA isolation

Total RNA was isolated using Trisure reagent (Bioline) following the manufacturer's instructions. Briefly, cells were washed twice with PBS and 1 ml Trisure was added for homogenization. After centrifuge, the aqueous phase was transferred to a new tube and mixed with cold isopropyl alcohol for RNA precipitation by centrifuging at 4 °C for 1 hour. RNA pellet was washed twice with 75% ethanol and finally dissolved in RNase-free water.

Reverse-transcription and quantitative real-time PCR (RT-qPCR)

Reverse transcription was performed with Tetro Reverse Transcriptase kit (Bioline) according to the manufacturer's instructions. Briefly, 2 μg total RNA was used as templates for each reaction. qPCR reactions were prepared using a SensiFAST SYBR No-ROX kit (Bioline) according to the instructions and performed in the Light Cycler 480 (Roche). Primers were listed in Table EV1.

Western blot analysis

Cells were washed twice with PBS and lysed with 2× SDS buffer (4% SDS, 20% glycerol and 125 mM Tris PH 6.8). Next, protein levels were quantified by Pierce BCA protein assay kit (Thermo Scientific). Lysates were loaded into a separating 7.5% SDS-PAGE gel and protein was transferred to nitrocellulose membranes. After blocking with 5% milk/PBS-Tween-20 (0.2%) solution, the membrane was incubated with mouse-anti-V5 (Thermo Fisher Scientific). Proteins were visualized using the secondary fluorescence-labeled antibodies goat-anti-mouse IRDye 680 RD (LI-COR Biosciences) and scanned on the Odyssey infrared imaging system (LI-COR Biosciences).

Immunofluorescence assay

Cells were grown on glass cover slips, washed twice with PBS and fixed with 2% PFA for 10 minutes at room temperature. Next, cells were permeabilized with 0.5% Triton/PBS solution, blocked with 5% FBS for 1 hour and incubated with mouse-anti-V5 (Thermo Fisher Scientific) and Alexa-488-conjugated Rabbit anti mouse secondary antibodies. Cover slips were mounted on glass slides using Vectashield containing DAPI. Images were taken with Leica confocal microscope SP5.

TruSeq standard mRNA sample preparation

Stranded-specific libraries were generated using the TruSeq Stranded mRNA sample preparation kit (Illumina) following the manufacturer's instructions. Briefly, 2 μg of total RNA was polyA-selected using oligo-dT beads and the RNA was fragmented, random primed and reverse transcribed using SuperScript II Reverse Transcriptase kit (Invitrogen). Second strand complementary DNA was then synthesized, 3'-adenylated and ligated to Illumina sequencing adapters, and subsequently amplified by 12 cycles of PCR. The sequencing libraries were analyzed on a 2100 Bioanalyzer using a 7500 chip (Agilent) and pooled equimolarly into a 30 nM multiplex sequencing pool.

Deep sequencing

Samples were sequenced on the Illumina HiSeq2500 sequencer generating 65-nuclotide single-end reads.

RNA-seq analysis

Sequenced reads were aligned to the human genome (hg19) using TopHat v2.0.8 (Trapnell *et al*, 2009). Only uniquely mapped reads were retained for further analysis. SAMTOOLS v0.1.19 (Li *et al*, 2009) was used to convert the BAM output to SAM format and to sort the BAM file. The read counts per gene were calculated using the HTSeq program, v0.5.4p1 (Anders *et al*, 2015). The DESeq package (Oshlack *et al*, 2010) was used to generate normalized read counts and for differential gene expression analysis. DESeq called differentially expressed genes with FDR cutoff of 0.05 and abs (FC) >1.5 were considered as significant differentially expressed genes.

IncuCyte® Caspase-3/7 Green apoptosis assay

Cells were pre-seeded in 96-well plate (Greiner, 655090) 48 hours before the addition of Caspase-3/7 Green Apoptosis reagent (Essen Bioscience, 4440). The green signals were captured every 4 hours and apoptotic cells were counted.

Animal studies

All mice experiments were approved by the Netherlands Cancer Institute Animal Experimental Committee. For Fig EV1E, xenografts were induced by subcutaneous injection of 4×10^6 PC3 control (sgNon-targeting) and sgSLC1A3 cells (monoclonal #4-1) in one flank of Balb/c nude mice (n=8) and treatment started when tumors reached 50 mm^3. For Fig 5A, 4×10^6 SUM159PT cells were resuspended in 50 μl PBS and injected into the mammary gland #4 of NOD-SCID IL2R-null (jax) (NSG) mice. After tumor volumes reached ~250 mm^3, mice (n=3 per group) were administrated either with mock (saline) or ASNase (60 U per day) for 5 consecutive days by intraperitoneal injections. Serum, mammary fat pad tissues and tumors were collected and snap-frozen for LC-MS analysis when the mice were sacrificed. For Fig 5B, 1×10^5 4T1 cells and 4T1-V5-SLC1A3 cells were respectively resuspended in 20 μl 1:1 mix of PBS and growth factor reduced Matrigel (Geltrex™, Gibco) and injected into 1 mammary fat pad per mouse. Mice were pre-treated for 2 days either with saline or ASNase (60 U per day) before tumor cells were introduced and the treatment was performed every day until the mice were sacrificed (n=13 per group except for the group of 4T1 treated with ASNase, n=12). Primary tumors were surgically removed once the tumor volumes reached 450–550 mm^3, and mice underwent breathing challenges every day. For Fig 5D, 5×10^4 MDA-MB-231 and MDA-MB-231-V5-SLC1A3 cells (in 50 μl PBS) were respectively injected into the tail veins of 2 days' pre-treated NSG mice (n=8 per group) and mice were sacrificed 22 days post tumor cells introduction.

All the experiments were using 6~8 weeks old NSG mice (except for Fig EV1E) and mice were weighed every 2 or 3 days to monitor weight loss. For ASNase treatment, mice were intraperitoneally administrated 60 U ASNase every day till the end of the experiments. Tumor volumes were calculated by the formula $V = 1/2(LW^2)$, where L is length and W is width of the primary tumor.

Histopathology analysis of lung and liver invasion

Lung and liver tissues were collected and fixed in formalin fixative and embedded in paraffin. The immunohistochemistry (IHC) of vimentin (DAKO, M0725, dilution: 1:4000) was conducted on 4μm-thick sections according to standard procedures. The stained slides were examined blindly by a pathologist and the number of tumorous lesions (more than 10 cancer cells) were scored in each of the sections. The sections were reviewed with a Zeiss Axioskop2 Plus microscope (Carl Zeiss Microscopy, Jena, Germany) and images were captured with a Zeiss AxioCam HRc digital camera and processed with AxioVision 4 software (both from Carl Zeiss Vision, München, Germany).

Statistics

Data analyses were performed using GraphPad Prism (version 7). The statistical tests used are described in figure legends. *p<0.05, **p<0.01, ***p<0.001. For the mass spectrometry analysis of amino acids in tumor samples, no statistics methods were used to predetermine sample size. For animal experiments, an estimate was made for the number of mice needed, without power calculation.

TCGA datasets analysis

Expression data from tumor and normal tissue samples were downloaded for every project available at ICGC data portal (http://dcc.icgc.org; release 27). For consistency, only expression data from pipeline “RNASeqV2_RSEM_genes” were considered. The downloaded normalized expression data were scaled to TPM (transcripts per million reads) and log2 transformed. Only projects with more than 10 normal samples were considered. All analyses were done using R-language. The statistical comparison between normal and tumor samples was done using a Wilcoxon sum rank test with Bonferroni correction for multiple comparisons.

Data availability

The deep sequencing datasets generated in this study have been deposited in GEO database under accession number: GSE134074. All other data generated that support the findings of this study are available from the corresponding author upon reasonable request.

Acknowledgements

We acknowledge all the members in Agami lab for valuable discussions. We thank Roderick Beijersbergen for providing the CRISPR-Cas9 library plasmid; Ron Kerkhoven, Roel Kluin and Iris de Rink from the NKI Genomics Core Facility for assisting with deep sequencing experiments and analysis. We appreciated the assistance from NKI Experimental Animal Pathology, Radionuclides Center and Flow cytometry facilities. We also thank the people from the Preclinical Intervention Unit and Pharmacology Unit of the Mouse Clinic for Cancer and Ageing (MCCA) at the NKI for performing the intervention studies. This work was supported by funds of the China Scholarship Council (201503250056) to J.S., the Dutch cancer society (KWF 0315/2016) and the European research council (ERC-PoC 665317) to R.A.

Author contributions

J.S. and R.A. conceived the project, designed the experiments and wrote the manuscript. J.S. performed most of the *in vitro* experiments for this project. R.N. provided technical support and established the protocols for the *in vivo* experiments. A.P.U. performed the bioinformatics analysis. E.A.Z. and C.R.B. performed metabolic mass-spectrometry experiments and analysed the data. R.H. helped with the RNA-seq library preparation. A.P. analysed RNA-seq data. A.B. and O.v.T. prepared materials for mice experiments. N.P. and M.v.d.V performed the in vivo experiments. H.F. and G.J.P. helped with the synthesis of TFB-TBOA. J.Y.S. performed histopathologic analysis. The project was supervised by R.A..

Conflict of interest

The authors declare that they have no conflict of interests.

References

Abrahamsen B, Schneider N, Erichsen MN, Huynh TH V., Fahlke C, Bunch L & Jensen AA (2013) Allosteric modulation of an excitatory amino acid transporter: the subtype-selective inhibitor UCPH-101 exerts sustained inhibition of EAAT1 through an intramonomeric site in the trimerization domain. *J. Neurosci.* **33:** 1068–1087 Available at: http://www.jneurosci.org/cgi/doi/10.1523/JNEUROSCI.3396-12.2013

Ahn CS & Metallo CM (2015) Mitochondria as biosynthetic factories for cancer proliferation. *Cancer Metab.* **3:** 1 Available at: https://cancerandmetabolism.biomedcentral.com/articles/10.1186/s40170-015-0128-2

Alkan HF, Walter KE, Luengo A, Madreiter-Sokolowski CT, Stryeck S, Lau AN, Al-Zoughbi W, Lewis CA, Thomas CJ, Hoefler G, Graier WF, Madl T, Vander Heiden MG & Bogner-Strauss JG (2018) Cytosolic Aspartate Availability Determines Cell Survival When Glutamine Is Limiting. *Cell Metab.* **28:** 706-720.e6 Available at: https://linkinghub.elsevier.com/retrieve/pii/S1550413118304649

Anders S, Pyl PT & Huber W (2015) HTSeq–a Python framework to work with high-throughput sequencing data. *Bioinformatics* **31:** 166–169 Available at: https://academic.oup.com/bioinformatics/article-lookup/doi/10.1093/bioinformatics/btu638

Avramis VI & Panosyan EH (2005) Pharmacokinetic/Pharmacodynamic Relationships of Asparaginase Formulations. *Clin. Pharmacokinet.* **44:** 367–393 Available at: http://link.springer.com/10.2165/00003088-200544040-00003

Bertero T, Oldham WM, Grasset EM, Bourget I, Boulter E, Pisano S, Hofman P, Bellvert F, Meneguzzi G, Bulavin D V., Estrach S, Feral CC, Chan SY, Bozec A & Gaggioli C (2019) Tumor-Stroma Mechanics Coordinate Amino Acid Availability to Sustain Tumor Growth and Malignancy. *Cell Metab.* **29:** 124-140.e10 Available at: https://doi.org/10.1016/j.cmet.2018.09.012

Broome JD (1961) Evidence that the L-Asparaginase Activity of Guinea Pig Serum is responsible for its Antilymphoma Effects. *Nature* **191:** 1114–1115 Available at: http://www.nature.com/articles/1911114a0

Bunpo P, Dudley A, Cundiff JK, Cavener DR, Wek RC & Anthony TG (2009) GCN2 Protein Kinase Is Required to Activate Amino Acid Deprivation Responses in Mice Treated with the Anti-cancer Agent l-Asparaginase. *J. Biol. Chem.* **284:** 32742–32749 Available at: http://www.jbc.org/lookup/doi/10.1074/jbc.M109.047910

Chan WK, Lorenzi PL, Anishkin A, Purwaha P, Rogers DM, Sukharev S, Rempe SB & Weinstein JN (2014) The glutaminase activity of L-asparaginase is not required for

anticancer activity against ASNS-negative cells. *Blood* **123:** 3596–3606 Available at: http://www.bloodjournal.org/cgi/doi/10.1182/blood-2013-10-535112

Chen J, Bardes EE, Aronow BJ & Jegga AG (2009) ToppGene Suite for gene list enrichment analysis and candidate gene prioritization. *Nucleic Acids Res.* **37:** W305–W311 Available at: https://academic.oup.com/nar/article-lookup/doi/10.1093/nar/gkp427

Chen S-H, Yang W, Fan Y, Stocco G, Crews KR, Yang JJ, Paugh SW, Pui C-H, Evans WE & Relling M V. (2011) A genome-wide approach identifies that the aspartate metabolism pathway contributes to asparaginase sensitivity. *Leukemia* **25:** 66–74 Available at: http://dx.doi.org/10.1038/leu.2010.256

Clarkson B, Krakoff I, Burchenal J, Karnofsky D, Golbey R, Dowling M, Oettgen H & Lipton A (1970) Clinical results of treatment with E. coli L-asparaginase in adults with leukemia, lymphoma, and solid tumors. *Cancer* **25:** 279–305 Available at: http://doi.wiley.com/10.1002/1097-0142%28197002%2925%3A2%3C279%3A%3AAID-CNCR2820250205%3E3.0.CO%3B2-7

Doench JG, Fusi N, Sullender M, Hegde M, Vaimberg EW, Donovan KF, Smith I, Tothova Z, Wilen C, Orchard R, Virgin HW, Listgarten J & Root DE (2016) Optimized sgRNA design to maximize activity and minimize off-target effects of CRISPR-Cas9. *Nat. Biotechnol.* **34:** 184–191 Available at: http://www.nature.com/doifinder/10.1038/nbt.3437

Garcia-Bermudez J, Baudrier L, La K, Zhu XG, Fidelin J, Sviderskiy VO, Papagiannakopoulos T, Molina H, Snuderl M, Lewis CA, Possemato RL & Birsoy K (2018) Aspartate is a limiting metabolite for cancer cell proliferation under hypoxia and in tumours. *Nat. Cell Biol.* **20:** 775–781 Available at: http://www.nature.com/articles/s41556-018-0118-z

Haskell CM, Canellos GP, Leventhal BG, Carbone PP, Block JB, Serpick AA & Selawry OS (1969) L-Asparaginase — Therapeutic and toxic effects in patients with neoplastic disease. *N. Engl. J. Med.* **281:** 1028–1034 Available at: https://doi.org/10.1056/NEJM196911062811902

Hays JL, Kim G, Walker A, Annunziata CM, Lee J, Squires J, Houston N, Steinberg SM & Kohn EC (2013) A phase II clinical trial of polyethylene glycol-conjugated L-asparaginase in patients with advanced ovarian cancer: Early closure for safety. *Mol. Clin. Oncol.* **1:** 565–569 Available at: http://www.ncbi.nlm.nih.gov/pubmed/24649212 [Accessed January 9, 2018]

Vander Heiden MG & DeBerardinis RJ (2017) Understanding the Intersections between Metabolism and Cancer Biology. *Cell* **168:** 657–669 Available at: http://dx.doi.org/10.1016/j.cell.2016.12.039

Hinze L, Pfirrmann M, Karim S, Degar J, McGuckin C, Vinjamur D, Sacher J, Stevenson KE, Neuberg DS, Orellana E, Stanulla M, Gregory RI, Bauer DE, Wagner FF, Stegmaier K & Gutierrez A (2019) Synthetic lethality of Wnt pathway activation and asparaginase in drug-resistant acute leukemias. *Cancer Cell* **35:** 664-676.e7 Available at: https://doi.org/10.1016/j.ccell.2019.03.004

Kanai Y, Clémençon B, Simonin A, Leuenberger M, Lochner M, Weisstanner M & Hediger MA (2013) The SLC1 high-affinity glutamate and neutral amino acid transporter family. *Mol. Aspects Med.* **34:** 108–120 Available at: https://linkinghub.elsevier.com/retrieve/pii/S0098299713000022

Kidd JG (1953) Regression of transplanted lymphomas induced in vivo by means of normal guinea pig serum. I. Course of transplanted cancers of various kinds in mice and rats given guinea pig serum, horse serum, or rabbit serum. *J. Exp. Med.* **98:** 565–582 Available at: http://www.jem.org/cgi/doi/10.1084/jem.98.6.565

Knott SR V., Wagenblast E, Khan S, Kim SY, Soto M, Wagner M, Turgeon M-O, Fish L, Erard N, Gable AL, Maceli AR, Dickopf S, Papachristou EK, D'Santos CS, Carey LA, Wilkinson JE, Harrell JC, Perou CM, Goodarzi H, Poulogiannis G, et al (2018) Asparagine bioavailability governs metastasis in a model of breast cancer. *Nature* **554:** 378–381 Available at: http://dx.doi.org/10.1038/nature25465

Korkmaz G, Lopes R, Ugalde AP, Nevedomskaya E, Han R, Myacheva K, Zwart W, Elkon R & Agami R (2016) Functional genetic screens for enhancer elements in the human genome using CRISPR-Cas9. *Nat. Biotechnol.* **34:** 192–198 Available at: http://www.nature.com/articles/nbt.3450

Krall AS, Xu S, Graeber TG, Braas D & Christofk HR (2016) Asparagine promotes cancer cell proliferation through use as an amino acid exchange factor. *Nat. Commun.* **7:** 11457 Available at: http://dx.doi.org/10.1038/ncomms11457

Li H, Handsaker B, Wysoker A, Fennell T, Ruan J, Homer N, Marth G, Abecasis G & Durbin R (2009) The Sequence Alignment/Map format and SAMtools. *Bioinformatics* **25:** 2078–2079 Available at: https://academic.oup.com/bioinformatics/article-lookup/doi/10.1093/bioinformatics/btp352

Li H, Ning S, Ghandi M, Kryukov G V., Gopal S, Deik A, Souza A, Pierce K, Keskula P, Hernandez D, Ann J, Shkoza D, Apfel V, Zou Y, Vazquez F, Barretina J, Pagliarini RA, Galli GG, Root DE, Hahn WC, et al (2019) The landscape of cancer cell line metabolism. *Nat. Med.* **25:** 850–860 Available at: http://www.nature.com/articles/s41591-019-0404-8

Li W, Xu H, Xiao T, Cong L, Love MI, Zhang F, Irizarry RA, Liu JS, Brown M & Liu XS (2014)

MAGeCK enables robust identification of essential genes from genome-scale CRISPR/Cas9 knockout screens. *Genome Biol.* **15:** 554 Available at: http://genomebiology.biomedcentral.com/articles/10.1186/s13059-014-0554-4

Loayza-Puch F, Rooijers K, Buil LCM, Zijlstra J, F. Oude Vrielink J, Lopes R, Ugalde AP, van Breugel P, Hofland I, Wesseling J, van Tellingen O, Bex A & Agami R (2016) Tumour-specific proline vulnerability uncovered by differential ribosome codon reading. *Nature* **530:** 490–494 Available at: http://dx.doi.org/10.1038/nature16982

Loayza-Puch F, Rooijers K, Zijlstra J, Moumbeini B, Zaal EA, Oude Vrielink JF, Lopes R, Ugalde AP, Berkers CR & Agami R (2017) TGFb1-induced leucine limitation uncovered by differential ribosome codon reading. *EMBO Rep.* **18:** 549–557 Available at: http://www.ncbi.nlm.nih.gov/pubmed/28274951 [Accessed January 11, 2018]

Müller H & J.Boos (1998) Use of L-asparaginase in childhood ALL. *Crit. Rev. Oncol. Hematol.* **28:** 97–113 Available at: https://linkinghub.elsevier.com/retrieve/pii/S1040842898000158

Nakamura A, Nambu T, Ebara S, Hasegawa Y, Toyoshima K, Tsuchiya Y, Tomita D, Fujimoto J, Kurasawa O, Takahara C, Ando A, Nishigaki R, Satomi Y, Hata A & Hara T (2018) Inhibition of GCN2 sensitizes ASNS-low cancer cells to asparaginase by disrupting the amino acid response. *Proc. Natl. Acad. Sci.* **115:** E7776–E7785 Available at: http://www.pnas.org/lookup/doi/10.1073/pnas.1805523115

Oshlack A, Robinson MD & Young MD (2010) From RNA-seq reads to differential expression results. *Genome Biol.* **11:** 220 Available at: http://genomebiology.biomedcentral.com/articles/10.1186/gb-2010-11-12-220

Pavlova NN, Hui S, Ghergurovich JM, Fan J, Intlekofer AM, White RM, Rabinowitz JD, Thompson CB & Zhang J (2018) As Extracellular Glutamine Levels Decline, Asparagine Becomes an Essential Amino Acid. *Cell Metab.* **27:** 428-438.e5 Available at: https://linkinghub.elsevier.com/retrieve/pii/S1550413117307167 [Accessed April 9, 2019]

Pui C-H, Campana D, Pei D, Bowman WP, Sandlund JT, Kaste SC, Ribeiro RC, Rubnitz JE, Raimondi SC, Onciu M, Coustan-Smith E, Kun LE, Jeha S, Cheng C, Howard SC, Simmons V, Bayles A, Metzger ML, Boyett JM, Leung W, et al (2009) Treating Childhood Acute Lymphoblastic Leukemia without Cranial Irradiation. *N. Engl. J. Med.* **360:** 2730–2741 Available at: https://doi.org/10.1056/NEJMoa0900386

Rabinovich S, Adler L, Yizhak K, Sarver A, Silberman A, Agron S, Stettner N, Sun Q, Brandis A, Helbling D, Korman S, Itzkovitz S, Dimmock D, Ulitsky I, Nagamani SCS, Ruppin E & Erez A (2015) Diversion of aspartate in ASS1-deficient tumours fosters de novo pyrimidine synthesis. *Nature* **527:** 379–383 Available at: http://dx.doi.org/10.1038/nature15529

Riccardi R, Holcenberg JS, Glaubiger DL, Wood JH & Poplack DG (1981) L-asparaginase pharmacokinetics and asparagine levels in cerebrospinal fluid of rhesus monkeys and humans. *Cancer Res.* **41:** 4554–4558 Available at: http://www.ncbi.nlm.nih.gov/pubmed/6895481

Scherf U, Ross DT, Waltham M, Smith LH, Lee JK, Tanabe L, Kohn KW, Reinhold WC, Myers TG, Andrews DT, Scudiero DA, Eisen MB, Sausville EA, Pommier Y, Botstein D, Brown PO & Weinstein JN (2000) A gene expression database for the molecular pharmacology of cancer. *Nat. Genet.* **24:** 236–244 Available at: http://www.nature.com/articles/ng0300_236

Shimamoto K, Sakai R, Takaoka K, Yumoto N, Nakajima T, Amara SG & Shigeri Y (2004) Characterization of novel L-threo-beta-benzyloxyaspartate derivatives, potent blockers of the glutamate transporters. *Mol. Pharmacol.* **65:** 1008–1015 Available at: http://molpharm.aspetjournals.org/lookup/doi/10.1124/mol.65.4.1008

Stams WAG (2003) Sensitivity to L-asparaginase is not associated with expression levels of asparagine synthetase in t(12;21)+ pediatric ALL. *Blood* **101:** 2743–2747 Available at: http://www.bloodjournal.org/cgi/doi/10.1182/blood-2002-08-2446

Sullivan LB, Gui DY, Hosios AM, Bush LN, Freinkman E & Vander Heiden MG (2015) Supporting Aspartate Biosynthesis Is an Essential Function of Respiration in Proliferating Cells. *Cell* **162:** 552–563 Available at: http://dx.doi.org/10.1016/j.cell.2015.07.017

Sullivan LB, Luengo A, Danai L V., Bush LN, Diehl FF, Hosios AM, Lau AN, Elmiligy S, Malstrom S, Lewis CA & Vander Heiden MG (2018) Aspartate is an endogenous metabolic limitation for tumour growth. *Nat. Cell Biol.* **20:** 782–788 Available at: http://www.nature.com/articles/s41556-018-0125-0

Tajan M, Hock AK, Blagih J, Robertson NA, Labuschagne CF, Kruiswijk F, Humpton TJ, Adams PD & Vousden KH (2018) A Role for p53 in the Adaptation to Glutamine Starvation through the Expression of SLC1A3. *Cell Metab.* **28:** 721-736.e6 Available at: https://www.sciencedirect.com/science/article/pii/S1550413118304480 [Accessed November 6, 2018]

Trapnell C, Pachter L & Salzberg SL (2009) TopHat: discovering splice junctions with RNA-Seq. *Bioinformatics* **25:** 1105–1111 Available at: https://academic.oup.com/bioinformatics/article-lookup/doi/10.1093/bioinformatics/btp120

Ueno T, Ohtawa K, Mitsui K, Kodera Y, Hiroto M, Matsushima A, Inada Y & Nishimura H (1997) Cell cycle arrest and apoptosis of leukemia cells induced by L-asparaginase. *Leukemia* **11:** 1858–1861 Available at: http://www.nature.com/articles/2400834

Van Vranken JG & Rutter J (2015) You Down With ETC? Yeah, You Know D! *Cell* **162:** 471–

473 Available at: http://dx.doi.org/10.1016/j.cell.2015.07.027

Ye J, Kumanova M, Hart LS, Sloane K, Zhang H, De Panis DN, Bobrovnikova-Marjon E, Diehl JA, Ron D & Koumenis C (2010) The GCN2-ATF4 pathway is critical for tumour cell survival and proliferation in response to nutrient deprivation. *EMBO J.* **29:** 2082–2096 Available at: http://dx.doi.org/10.1038/emboj.2010.81

Expanded View Figures

Figure EV1

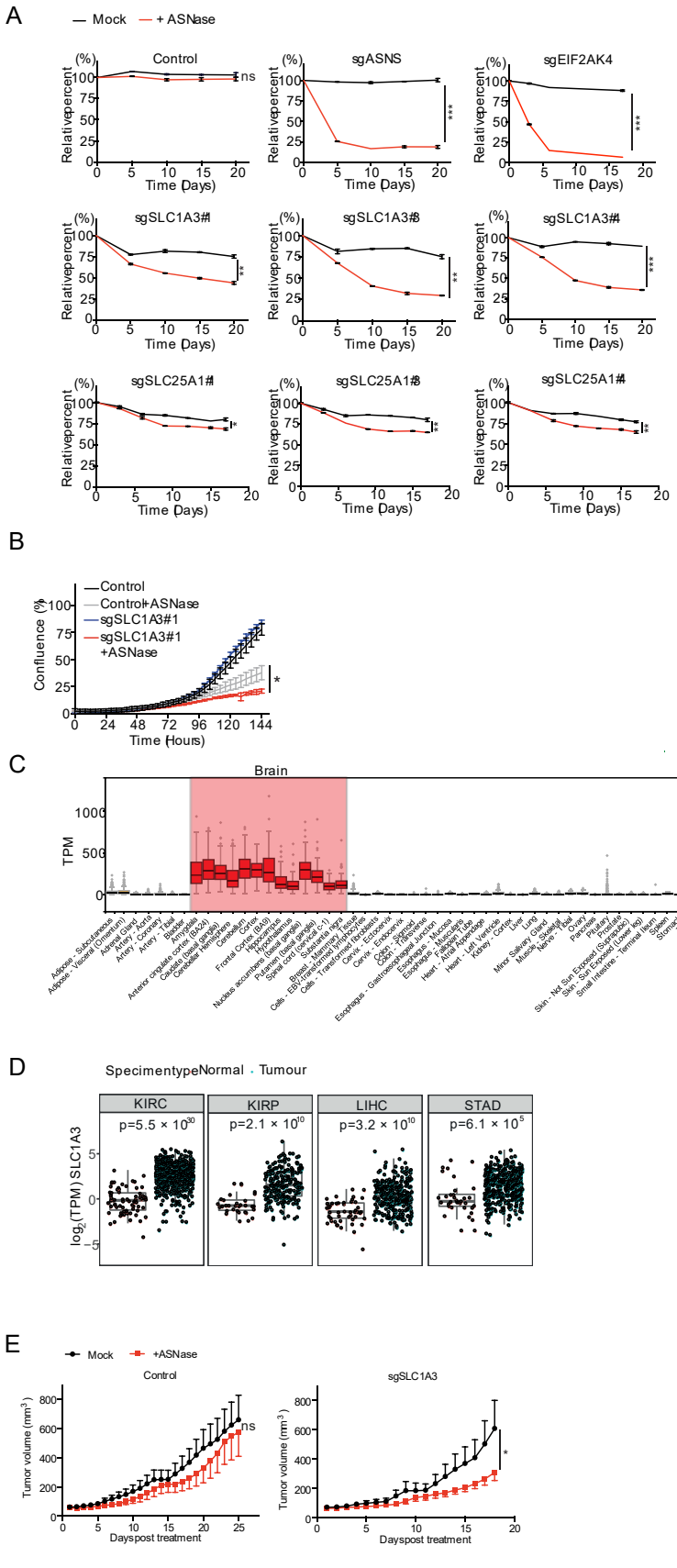
A
Mock
+ASNase
Control
sgASNS
sgEIF2AK4
sgSLC1A3#1
sgSLC1A3#3
sgSLC1A3#4
sgSLC25A1#1
sgSLC25A1#3
sgSLC25A1#4
Relativepercent
Time Days
ns
B
Control
Control+ASNase
sgSLC1A3#1
sgSLC1A3#1 +ASNase
Confluence (%)
Time (Hours)
C
Brain
TPM
D
SpecimentypeNormal
Tumour
KIRC
KIRP
LIHC
STAD
p=5.5 × 10^30
p=2.1 × 10^10
p=3.2 × 10^10
p=6.1 × 10^5
log2(TPM) SLC1A3
E
Mock
+ASNase
Control
sgSLC1A3
Tumor volume (mm3)
Dayspost treatment

Figure EV1. Validation of hits from the genome-wide CRISPR-Cas9 screen in PC3 cells.

A. PC3 cells were transduced with individual sgRNA lentiviral vectors as indicated and subjected to competitive cell proliferation assays under mock or ASNase (0.3 U/ml) conditions. #1, #3 and #4 represent different sgRNAs and n=2 for each condition.
B. PC3 cells were transduced with control (sgNon-targeting) or sgSLC1A3 and subjected to IncuCyte cell proliferation assays with or without ASNase (0.3 U/ml). #1 indicates a sgRNA targeting SLC1A3 and n=3 for each condition
C. SLC1A3 expression analysis in normal tissues from GTEX portal (gtexportal.org/home/gene/SLC1A3). Red columns indicate high SLC1A3 expression in most brain tissues. Expression values are shown in TPM (transcripts Per Million), calculated from a gene model with isoforms collapsed to a single gene. No other normalization steps have been applied. Box plots are shown as median and 25th and 75th percentiles; points are displayed as outliers if they are above or below 1.5 times the interquartile range.
D. TCGA tumor database analysis of SLC1A3 expression in healthy tissues and primary tumors for kidney renal clear cell carcinoma (KIRC), kidney renal papillary cell carcinoma (KIRP), liver hepatocellular carcinoma (LIHC) and stomach adenocarcinoma (STAD). Expression data from tumor and normal tissue samples were downloaded fro every project available at ICGC data portal (http://dcc.icgc.org; release 27). For consistency, only expression data from pipeline "RNASeqV2_RSEM_genes" were considered. The downloaded normalized expression data were scaled to TPM (transcripts per million reads) and log2 transformed. Only projects with more than 10 normal samples were considered (each dot represents one sample). All analyses were done using R-language. The statistical comparison between normal and tumor samples was done using a non-parametric Wilcoxon sum rank test followed by Bonferroni correction. Box plots are shown as median and 25th and 75th percentiles; points are displayed as outliers if they are above or below 1.5 times the interquartile range.
E. Control (sgNon-targeting#1) and SLC1A3 knockout (sgSLC1A3#4-1) PC3 cell lines were subcutaneously injected into Balb/c nude mice (cAnN/Rj) (n=8 per group). Once tumor volumes reached 50 mm^3, mice were treated with mock (saline) or ASNase (60 U per day). Data was presented as mean ± SEM.

Data information: Results were presented as mean ± SD, unless otherwise stated. The *p*-value was calculated by two-tailed unpaired t test from Prism7. **p*<0.05, ***p*<0.01, ****p*<0.001.

Figure EV2

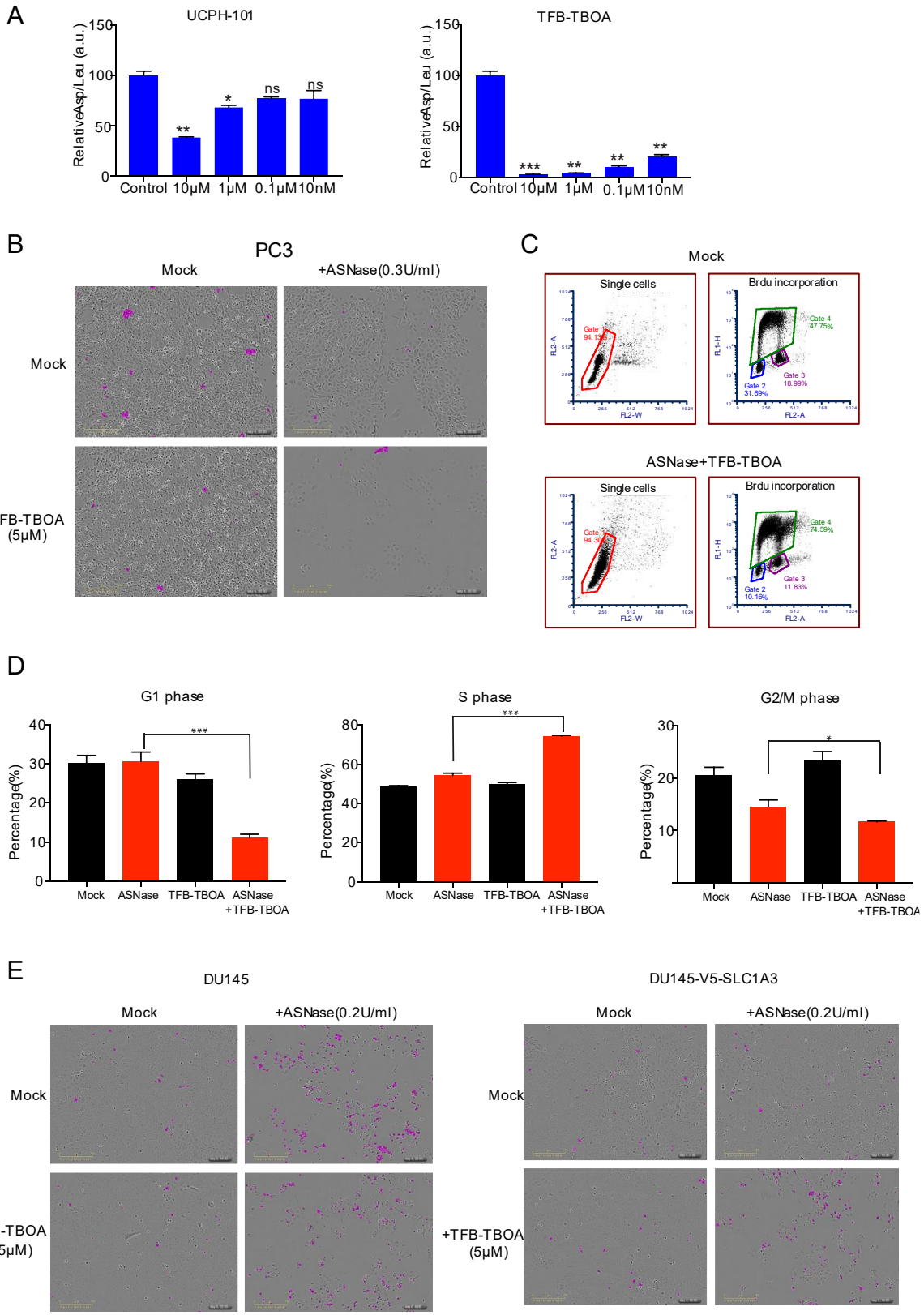
A
UCPH-101
TFB-TBOA
RelativeAsp/Leu (a.u.)
Control 10μM 1μM 0.1μM 10nM
B
PC3
Mock
+ASNase(0.3U/ml)
+TFB-TBOA (5μM)
C
Mock
Single cells
Brdu incorporation
ASNase+TFB-TBOA
D
G1 phase
S phase
G2/M phase
Percentage(%)
Mock ASNase TFB-TBOA ASNase +TFB-TBOA
E
DU145
DU145-V5-SLC1A3
Mock
+ASNase(0.2U/ml)
+TFB-TBOA (5μM)

F

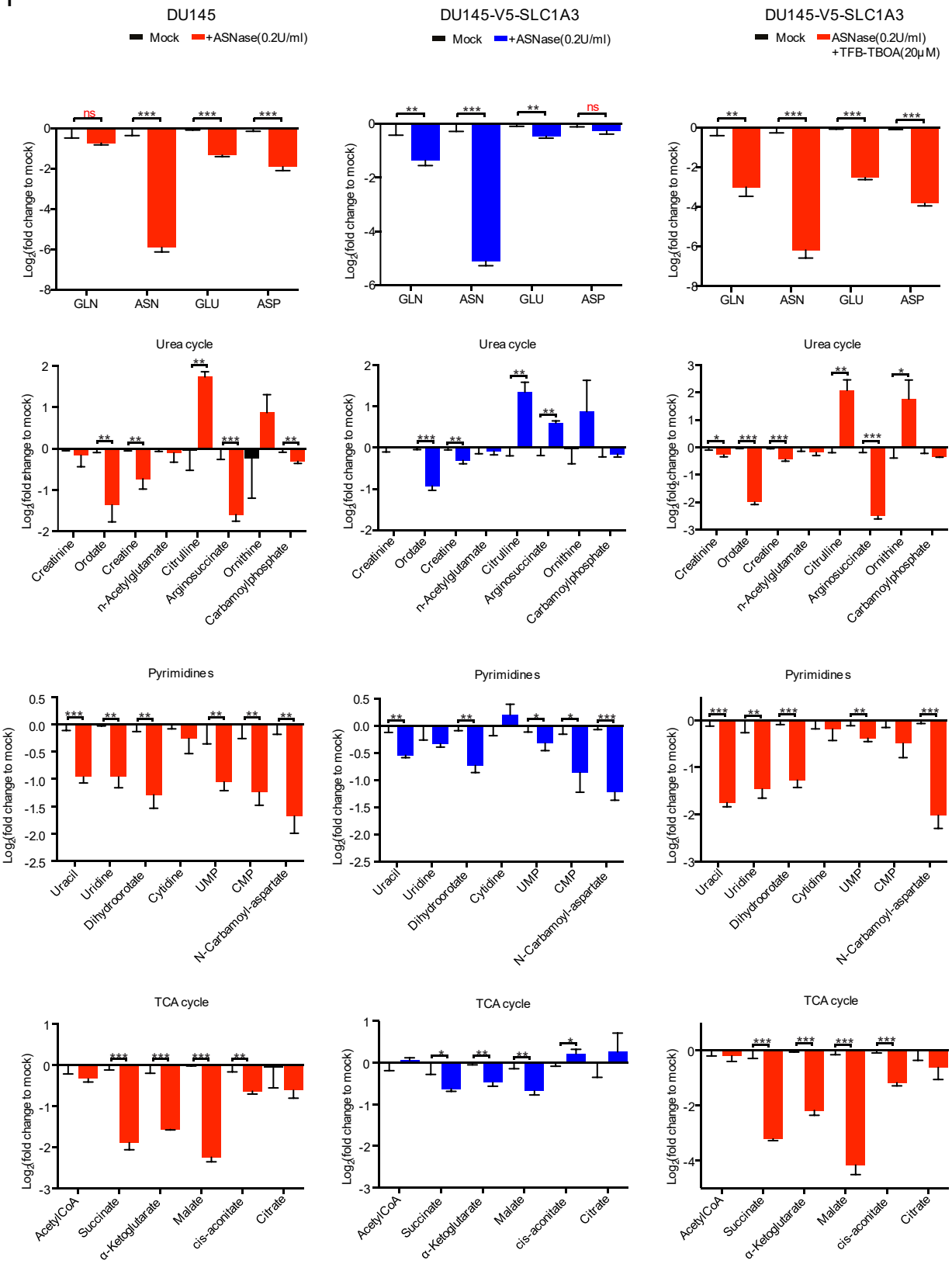
DU145
Mock
+ASNase(0.2U/ml)
DU145-V5-SLC1A3
Mock
+ASNase(0.2U/ml)
DU145-V5-SLC1A3
Mock
ASNase(0.2U/ml)
+TFB-TBOA(20μM)
Log2(fold change to mock)
GLN
ASN
GLU
ASP
Urea cycle
Creatinine
Orotate
Creatine
n-Acetylglutamate
Citrulline
Arginosuccinate
Ornithine
Carbamoylphosphate
Pyrimidines
Uracil
Uridine
Dihydroorotate
Cytidine
UMP
CMP
N-Carbamoyl-aspartate
TCA cycle
AcetylCoA
Succinate
α-Ketoglutarate
Malate
cis-aconitate
Citrate

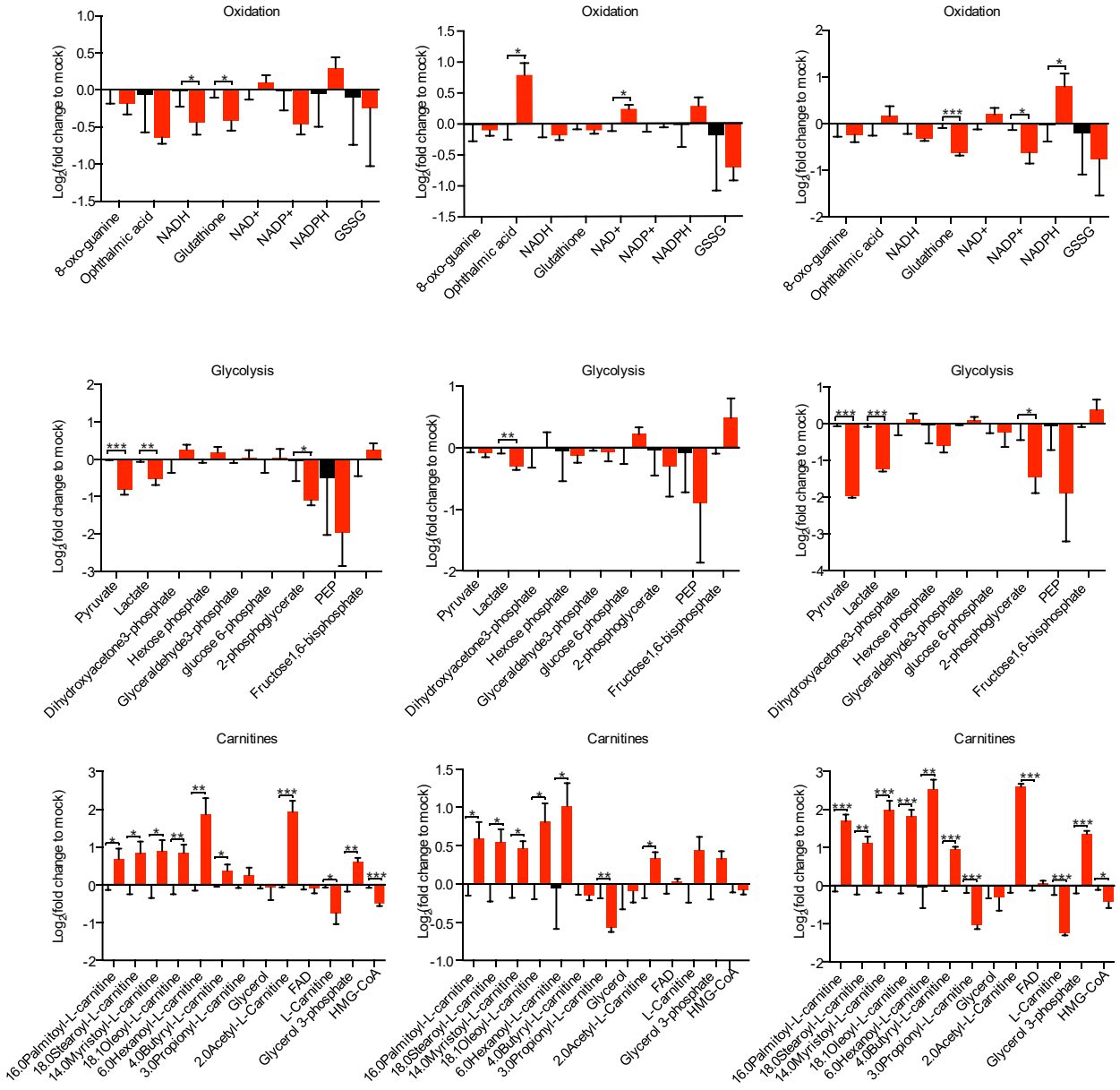

Figure EV2. Combination of ASNase and SLC1A3 inhibition impairs cancer cell proliferation.

A. PC3 cells were incubated with two SLC1A3 inhibitors (UCPH-101 and TFB-TBOA) at indicated concentrations and subjected to an aspartate uptake assay (n=2). Leucine uptake level was used for normalization.

B. PC3 cells were treated with ASNase (0.3 U/ml) and TFB-TBOA (5 μM) as indicated and images were taken after 4 days. The scale bar indicates 300 μm and cells highlighted in pink present apoptotic cells.

C. PC3 cells were treated with mock or combination of ASNase (0.3 U/ml) and TFB-TBOA (5 μM) for 9 days and subjected to flow cytometry measurements of cell cycle using BrdU labelling.

D. Flow cytometry cell cycle distribution analysis of PC3 cells under indicated conditions for 9 days by BrdU labeling. ASNase (0.3 U/ml) and TFB-TBOA (5 μM).
E. Representative images of apoptosis in DU145 and DU145-V5-SLC1A3 cells treated with ASNase (0.2 U/ml) and TFB-TBOA (5 μM) as indicated, and subjected to IncuCyte analysis for apoptotic cells (highlighted in pink). The scale bar indicates 300 μm.
F. DU145 and DU145-V5-SLC1A3 cells were treated with ASNase (0.2 U/ml) and TFB-TBOA (20 μM) for 3 days as indicated, and collected for metabolome analysis by LC-MS to determine the relative levels of amino acids and metabolites involved in urea cycle, pyrimidines synthesis, TCA cycle, oxidation, glycolysis and carnitines. GLN: glutamine; ASN: asparagine; GLU: glutamate; ASP: aspartate; TCA cycle: tricarboxylic acid cycle; UMP: uridine monophosphate; CMP: cytidine monophosphate; PEP: phosphoenolpyruvate; NADH: nicotinamide adenine dinucleotide (reduced form); NAD^+: nicotinamide adenine dinucleotide (oxidized form); NADPH: nicotinamide adenine dinucleotide phosphate (reduced form); $NADP^+$: nicotinamide adenine dinucleotide phosphate (oxidized form); GSSG: glutathione disulfide; HMG-CoA: 3-hydroxy-3-methylglutaryl-CoA; FAD: flavin adenine dinucleotide.

Data information: Results were calculated based on three independent replicates, unless otherwise stated, and presented as mean ± SD. The *p*-value was calculated by two-tailed unpaired t test from Prism7. **p*<0.05, ***p*<0.01, ****p*<0.001.

Figure EV3

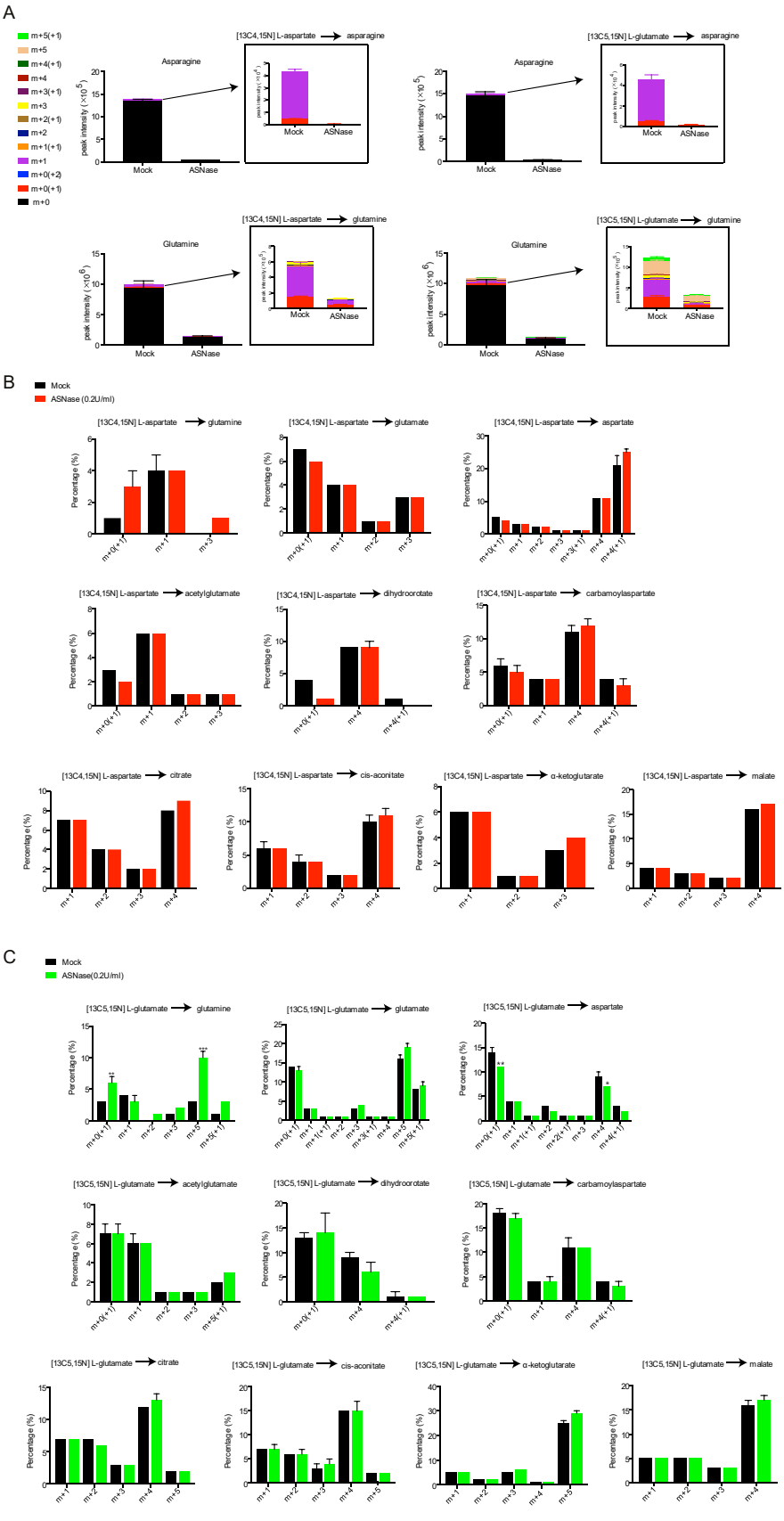
A
m+5(+1)
m+5
m+4(+1)
m+4
m+3(+1)
m+3
m+2(+1)
m+2
m+1(+1)
m+1
m+0(+2)
m+0(+1)
m+0
[13C4,15N] L-aspartate → asparagine
[13C5,15N] L-glutamate → asparagine
[13C4,15N] L-aspartate → glutamine
[13C5,15N] L-glutamate → glutamine
Asparagine
Glutamine
peak intensity (×10^5)
peak intensity (×10^6)
Mock
ASNase
B
Mock
ASNase (0.2U/ml)
[13C4,15N] L-aspartate → glutamine
[13C4,15N] L-aspartate → glutamate
[13C4,15N] L-aspartate → aspartate
[13C4,15N] L-aspartate → acetylglutamate
[13C4,15N] L-aspartate → dihydroorotate
[13C4,15N] L-aspartate → carbamoylaspartate
[13C4,15N] L-aspartate → citrate
[13C4,15N] L-aspartate → cis-aconitate
[13C4,15N] L-aspartate → α-ketoglutarate
[13C4,15N] L-aspartate → malate
Percentage (%)
C
Mock
ASNase(0.2U/ml)
[13C5,15N] L-glutamate → glutamine
[13C5,15N] L-glutamate → glutamate
[13C5,15N] L-glutamate → aspartate
[13C5,15N] L-glutamate → acetylglutamate
[13C5,15N] L-glutamate → dihydroorotate
[13C5,15N] L-glutamate → carbamoylaspartate
[13C5,15N] L-glutamate → citrate
[13C5,15N] L-glutamate → cis-aconitate
[13C5,15N] L-glutamate → α-ketoglutarate
[13C5,15N] L-glutamate → malate
Percentage (%)

Figure EV3. Isotopic tracing of aspartate and glutamate in DU145-V5-SLC1A3 cells.

DU145-V5-SLC1A3 cells were pretreated with ASNase (0.2 U/ml) for 48hrs and then supplemented with [$^{13}C_4$,^{15}N] L-aspartate (1.5mM) and unlabeled glutamate (1.5mM), or [$^{13}C_5$,^{15}N] L-glutamate (1.5mM) and unlabeled aspartate (1.5mM) for 8 hrs. Subsequently, cells were harvested for LC-MS analysis.

A. Mass isotopologue analysis of ^{13}C and ^{15}N incorporation into asparagine and glutamine in DU145-V5-SLC1A3 cells cultured as indicated conditions.
B. Mass isotopologue analysis of ^{13}C and ^{15}N incorporation into glutamine, glutamate and aspartate and metabolites from TCA cycle, urea cycle and nucleotide synthesis in DU145-V5-SLC1A3 cells cultured with [$^{13}C_4$,^{15}N] L-aspartate and unlabeled glutamate.
C. Mass isotopologue analysis of ^{13}C and ^{15}N incorporation into glutamine, glutamate and aspartate and metabolites from TCA cycle, urea cycle and nucleotide synthesis in DU145-V5-SLC1A3 cells cultured with [$^{13}C_5$,^{15}N] L-glutamate and unlabeled aspartate.

Data information: Data shown in (B–C) were calculated as labeled fraction divided by total peak area (including unlabeled fraction) and results were presented as mean ± SD (n=3). Number before brackets accounts for ^{13}C incorporation and number in brackets accounts for ^{15}N incorporation. The *p*-value was calculated by two-tailed unpaired t test from Prism7. **p*<0.05, ***p*<0.01, ****p*<0.001.

Figure EV4

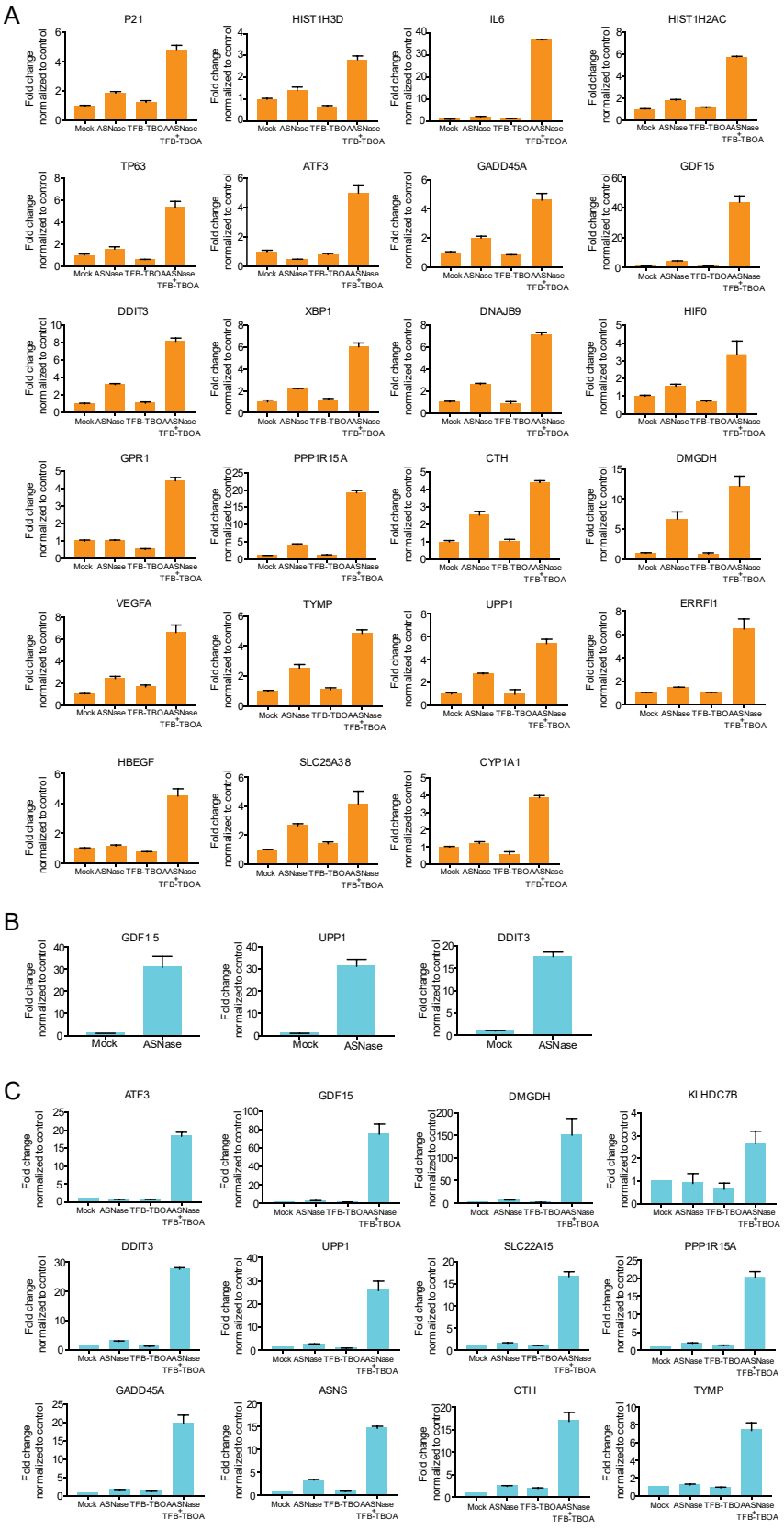
A
P21
HIST1H3D
IL6
HIST1H2AC
TP63
ATF3
GADD45A
GDF15
DDIT3
XBP1
DNAJB9
HIF0
GPR1
PPP1R15A
CTH
DMGDH
VEGFA
TYMP
UPP1
ERRFI1
HBEGF
SLC25A38
CYP1A1
Fold change normalized to control
Mock ASNase TFB-TBOA ASNase + TFB-TBOA
B
GDF15
UPP1
DDIT3
Mock
ASNase
C
ATF3
GDF15
DMGDH
KLHDC7B
DDIT3
UPP1
SLC22A15
PPP1R15A
GADD45A
ASNS
CTH
TYMP

Figure EV4. RT-qPCR validation of differential expressed genes in PC3, DU145 and DU145-V5-SLC1A3 Cells from Figure 4.

A–C. RT-qPCR validation based on transcriptome analysis in PC3 (A), DU145 (B) and DU145-V5-SLC1A3 cells (C).

Data information: Results were calculated based on three independent replicates, and presented as mean ± SD.

Figure EV5

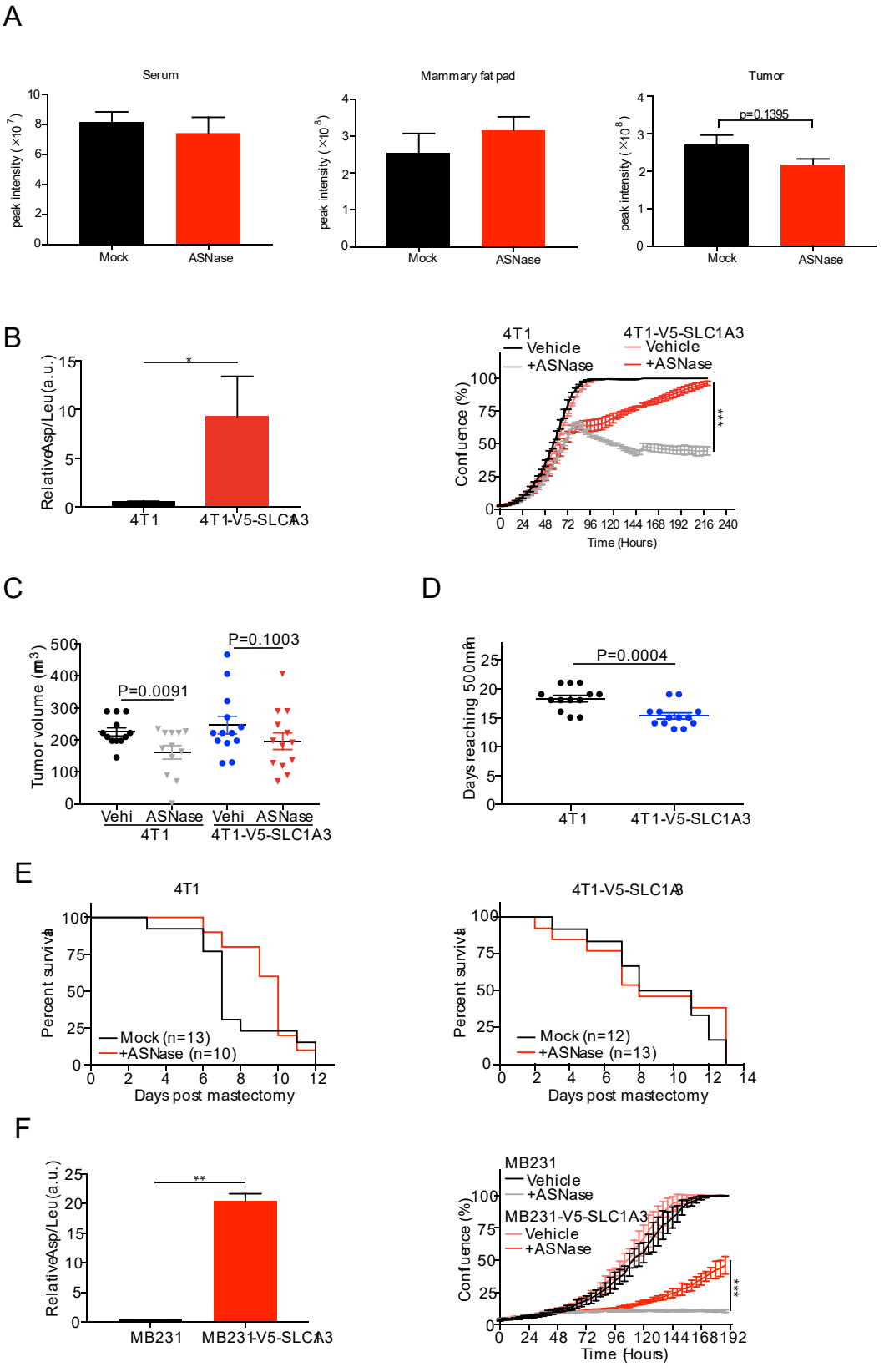
A
Serum
Mammary fat pad
Tumor
peak intensity (×10^7)
peak intensity (×10^8)
p=0.1395
Mock
ASNase
B
Relative Asp/Leu (a.u.)
*
4T1
4T1-V5-SLC1A3
4T1
Vehicle
+ASNase
4T1-V5-SLC1A3
Vehicle
+ASNase
Confluence (%)
***
Time (Hours)
C
Tumor volume (mm^3)
P=0.0091
P=0.1003
Vehi
ASNase
4T1
4T1-V5-SLC1A3
D
Days reaching 500mm^3
P=0.0004
E
4T1
4T1-V5-SLC1A3
Percent survival
Mock (n=13)
+ASNase (n=10)
Mock (n=12)
+ASNase (n=13)
Days post mastectomy
F
Relative Asp/Leu (a.u.)
**
MB231
MB231-V5-SLC1A3
MB231
Vehicle
+ASNase
MB231-V5-SLC1A3
Vehicle
+ASNase
Confluence (%)
***
Time (Hours)

Figure EV5. SLC1A3 expression promotes ASNase resistance and tumor progression *in vivo*.

A. Glutamine levels in serum, mammary fat pad tissues and growing tumors derived from SUM159PT human breast cancer cells with or without ASNase treatment (60 U per day) for consecutive 5 days. Essential amino acids were used for the raw data normalization. Results were presented as mean ± SEM (n=3).

B. Left: quantification of aspartate uptake in parental 4T1 and 4T1-V5-SLC1A3 cells (n=2). Leucine uptake was used for normalization. The *p*-value was calculated by one-tailed unpaired t test in Prism7.
   Right: IncuCyte cell proliferation curves for parental 4T1 and 4T1-V5-SLC1A3 cells with or without ASNase (0.2 U/ml) for 10 days (n=3).

C. Tumor volumes resulting from orthotopic implantation of parental 4T1 and 4T1-V5-SLC1A3 cells at day 12 (n=13 mice per group, except for 4T1+ASNase, n=12). Results were presented as mean ± SEM.

D. Days for orthotopically injected parental 4T1 and 4T1-V5-SLC1A3 cells to reach 450–550 mm^3. Results were presented as mean ± SEM (n=13).

E. Following the mastectomy, mice were daily challenged for breathing test and sacrificed due to breathing problems. The survival rate for 4T1 and 4T1-V5-SLC1A3 injected mice was scored in Prism7.

F. Left: quantification of aspartate uptake in MDA-MB-231 and MDA-MB-231-V5-SLC1A3 cells (n=2). Leucine uptake was used for normalization.
   Right: IncuCyte cell proliferation measurements for MDA-MB-231 and MDA-MB-231-V5-SLC1A3 cells with or without ASNase (1 U/ml) for 8 days (n=3).

Data information: Results were calculated based on three replicates and presented as mean ± SD (unless otherwise stated). The *p*-value was calculated by two-tailed unpaired t test except for (B) in Prism7. **p*<0.05, ***p*<0.01, ****p*<0.001.

Chapter 4
PYCR1 inhibition for cancer treatment

Kirsty Milne[a], Jianhui Sun[b], Esther A. Zaal[c], Jenna Mowat[a], Patrick H.N. Celie[b,d], Alexander Fish[b,d], Celia R. Berkers[c,e], Giuseppe Forlani[f], Fabricio Loayza-Puch[b], Craig Jamieson[a], Reuven Agami[b,g]

[a] Department of Pure and Applied Chemistry, Thomas Graham Building, University of Strathclyde, Glasgow G1 1XL, United Kingdom
[b] H5 Division of Oncogenomics, Oncode Institute, The Netherlands Cancer Institute, 121 Plesmanlaan, 1066 CX Amsterdam, The Netherlands
[c] Biomolecular Mass Spectrometry and Proteomics, Bijvoet Center for Biomolecular Research, Utrecht University, Padualaan 8, 3584 CH Utrecht, The Netherlands
[d] NKI Protein Facility, Division of Biochemistry, The Netherlands Cancer Institute, 121 Plesmanlaan, 1066 CX Amsterdam, The Netherlands
[e] Department of Biochemistry and Cell Biology, Faculty of Veterinary Medicine, Utrecht University, Yalelaan 2, 3584 CM Utrecht, The Netherlands
[f] Department of Life Science and Biotechnology, University of Ferrara, 44121 Ferrara, Italy
[g] Department of Molecular Genetics, Erasmus MC, Rotterdam University, The Netherlands

Adapted from Bioorganic & Medicinal Chemistry Letters 29 (2019): 2626-2631.

Abstract

Pyrroline-5-carboxylate reductase 1 (PYCR1) is the final enzyme involved in the biosynthesis of proline and has been found to be upregulated in various forms of cancer. Due to the role of proline in maintaining the redox balance of cells and preventing apoptosis, PYCR1 is emerging as an attractive oncology target. Previous PYCR1 knockout studies led to a reduction in tumor growth. Accordingly, a small molecule inhibitor of PYCR1 could lead to new treatments for cancer, and a focused screening effort identified pargyline as a fragment-like hit. We report the design and synthesis of the first tool compounds as PYCR1 inhibitors, derived from pargyline, which were assayed to assess their ability to attenuate the production of proline. Structural activity studies have revealed the key determinants of activity, with the most potent compound

(4) showing improved activity *in vitro* in enzyme (IC_{50} = 8.8 μM) and pathway relevant effects in cell-based assays.

Pyrroline-5-carboxylate reductase 1 (PYCR1) is the final enzyme involved in the biosynthesis of proline from both glutamic acid and ornithine, as outlined in scheme 1 (Christensen *et al*, 2017a). Glutamic acid is firstly phosphorylated by glutamate 5-kinase (G5K), before being dephosphorylated by gamma-glutamyl phosphate reductase (γ-GPR) to produce glutamate-γ-semialdehyde, which exists in an equilibrium with pyrroline-5-carboxylate (P5C). Ornithine is also transformed to the same intermediate through the action of ornithine amino transferase (OAT). P5C is then finally reduced to proline by PYCR1 using the reduced form of nicotinamide adenine dinucleotide phosphate (NADPH) as a cofactor, although *in vitro* nicotinamide adenine dinucleotide (NADH) can also serve as a co-factor.

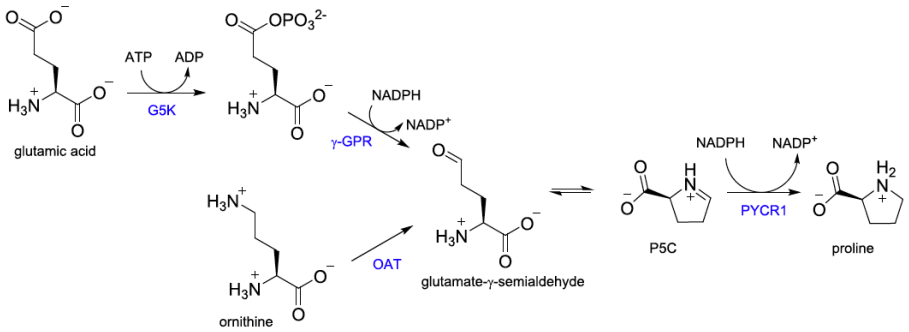

Scheme 1. The proline biosynthesis pathway (adapted from (Christensen *et al*, 2017b)).

Proline is essential for protein synthesis and plays a role in the secondary structure of proteins. This amino acid and its derivatives are also the main residues found in collagen, the most abundant protein found within the body (Phang *et al*, 2008). However, it also plays a role in maintaining the redox balance of cells through a process known as the proline cycle (Phang *et al*, 2008; Liang *et al*, 2013; Tanner *et al*, 2018).

P5C is regenerated in the mitochondria by the oxidation of proline by proline dehydrogenase (PRODH), generating adenosine triphosphate (ATP), in the process. Outside of the mitochondria, P5C can be reconverted to proline. This produces a molecule of nicotinamide adenine dinucleotide phosphate (NADP+) which is available for use by the pentose-phosphate pathway. The pentose-phosphate pathway will eventually produce ribose-5-phosphate (R-5-P), which can be used to synthesize nucleotides or undergo further transformations to eventually

reach fructose-6-phosphate (F-6-P), that is able to produce ATP through glycolysis. These three process have an essential role in the survival and proliferation of cells (Song *et al*, 2016; Lane & Fan, 2015; Kim *et al*, 2018). The pentose-phosphate pathway also reduces NADP+ back to NADPH which then supports the disulfide reduction system via thioredoxin reductase and glutathione reductase, minimizing production of reactive oxygen species (ROS), again contributing to cell survival.

In healthy cells, these processes are highly regulated and essential for maintaining normal function (Tanner *et al*, 2018). However, in certain cancers, such as breast, prostate and some lung and skin cancers, PYCR1 is found to be upregulated (Craze *et al*, 2018; Cai *et al*, 2018; Ding *et al*, 2017; de Ingeniis *et al*, 2012; Zeng *et al*, 2017). This leads to higher levels of proline and exacerbated effects of the proline cycle, with the cells effectively using this method to increase cell survival (Tanner *et al*, 2018). If a method of reducing or inhibiting PYCR1 activity could be discovered, it could provide a new means of treating cancer. We and others have reported studies in both breast cancer (Loayza-Puch *et al*, 2016) and human prostate (Zeng *et al*, 2017) cell lines showing that PYCR1 knockout causes phenotypic changes in the cell. In the prostate cancer studies, this resulted in an increase in cell cycle arrest and apoptosis *in vitro*, while in the breast cancer studies a reduction in tumor size *in vivo* was observed. These experiments have shown that modulating PYCR1 directly affects the survival rate of some cancers, validating PYCR1 as an emerging oncology target.

While omission of a gene is a useful tool in its own right, the process is complex and careful selection of vectors and delivery vehicles are required to minimize inflammatory and off-target effects, which can make the process lengthy and expensive (Selkirk, 2004; Kang *et al*, 2016; Liang *et al*, 2015). Furthermore, gene therapy is not yet an officially approved treatment for any disease and until more is known about the human genome, this is not likely to be approved in the near future (Petropoulos *et al*, 2016). A more tractable approach would utilize a small molecule tool compound, potentially leading to a new approved therapy for cancer treatment.

In order to identify a chemical starting point, a commercially available library of pharmaceutically active compounds (LOPAC®1280, Sigma Aldrich) was screened against PYCR1. Based on this screening campaign, pargyline was identified as a fragment-like hit (1, Fig. 1). Pargyline had a modest IC_{50} of 198 μM, however, displayed an encouraging ligand efficiency (LE) of 0.42 (Chen *et al*, 2015).

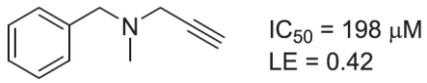

1

Fig. 1. Structure and activity of pargyline.

These considerations, coupled with its low molecular weight, made it an attractive fragment-like hit and a number of analogues were prepared in order to assess the structure activity relationship (SAR). Starting from the appropriate amine, the target analogues were synthesized via alkylation or reductive amination with the corresponding bromide or aldehyde, respectively, as outlined in Scheme 2.

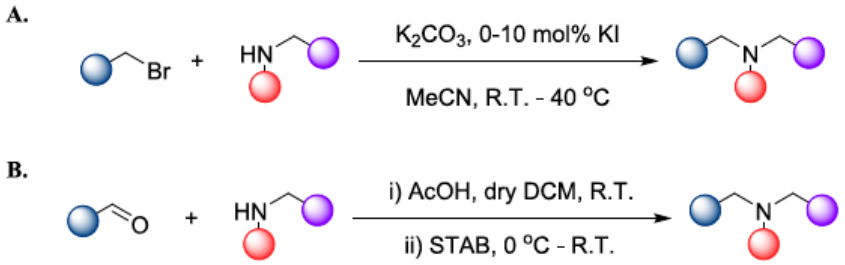

Scheme 2. A: Alkylation conditions; bromide (0.25 mmol), amine (0.25 mmol), acetonitrile (0.8 M), with potassium iodide added for less activated bromides. B: Reductive amination conditions; aldehyde (3 mmol), amine (1 mmol), acetic acid (1 mmol), dry dichloromethane (0.05 M) then sodium triacetoxyborohydride (3 mmol).

The modular structure of pargyline makes it amenable to targeted elaboration of three principal regions: the benzyl, N-methyl and propargyl groups. As no crystallographic information of the binding site pargyline occupies within PYCR1 was available, a stepwise approach was adopted in order to assess the impact of changing these substituents on enzyme inhibition using the *in vitro* compound screening assay.

Initially, changes to the benzyl group were examined. Due to their relative abundance in pharmaceutically active compounds, the presence of halogens in various positions around the phenyl ring of the benzyl group was assessed first (Fig. 2A) (Ford & Ho, 2016). Pleasingly almost all of the compounds were found to be more active than pargyline in PYCR1 inhibition, with the exception of the 4-fluoro, 2-chloro and 2-bromo derivatives (2, 8 and 9, respectively) which showed reduced activity. It was also found that the influence on activity was greatest when the halogen was in the 4-position (3–5) and weakest in the 2-position (7 and 9), with the 3-position being between the two potencies (6 and 7). The size of the halogen in the 4-position

was also found to have an effect with a general increase in potency observed moving down the group (2–5), with the optimum being the 4-bromo system, which was very similar in potency to the 4-iodo moiety, with both of these surpassing the 4-chloro derivative.

In order to follow up on these observations, a number of different functional groups on the benzyl ring were studied, as shown in Fig. 2B. A range of electron donating and withdrawing groups were analyzed in various positions around the ring. Again, the 4-position was favored with a similar pattern of activity being observed with the nitro group (14–16) as with the halogens. Unfortunately, none of the compounds matched the potency of compound 4, with no clear preference for electron donating (10–12) or withdrawing groups (13–18) noted from this study.

With more potent analogues observed with increasing size of halogen, it was reasoned that larger groups on the benzyl ring could also result in an increase in potency. Due to the similarities in volume of iodine and phenyl moieties (Stepan *et al*, 2012), some biphenyls (19 and 20) were prepared by Suzuki coupling of compound 4. Unfortunately, these analogues were less active than both pargyline and compound 4, suggesting that there are other properties beyond the size of substituent contributing to the increase in potency. This could be linked to a halogen bonding effect, where the strength of an interaction increases with the size of the halogen atom, as observed with analogues 2–4 (Ford & Ho, 2016).

Compound 4 was found to have the highest potency, also improving the LE, showing that the presence of a bromine atom on the 4-position of the benzyl group may be beneficial to binding. With the previous exemplars only representing a single substitution on the benzyl group, it was decided to incorporate a variety of disubstituted analogues as shown in Fig. 2C. Initially, this was probed using dichlorobenzyl moieties due to their synthetic availability. In comparison to compound 3, having substitution of the 3- and 4-positions resulted in a compound with a similar potency to the monosubstituted 4-position, while the 3,5- and 2,6- derivatives (compounds 23 and 24, respectively) were inactive.

Exchanging the 3-chloro of compound 22 for a trifluoromethyl group (21) resulted in a less active compound, again suggesting the importance of halogens. However, the 2,4-dichloro species 25 had a much greater potency than compound 3 and a similar potency to compound 4. This was surprising as a monosubstituted compound in the 2-position was found to be the least

active regioisomer in the initial halogen screen (7 and 9). This increase in potency could be due to an extra interaction at the, as yet unknown, binding site of the enzyme which complements the interaction at the 4-position. Other disubstituted modifications (26–34) and naphthyl (25) resulted in lower levels of activity.

The final modifications to the benzyl group involved exchanging it for a completely different functional handle to assess its necessity for activity, as outlined in Fig. 2D. Homologation (36) and exchange of the 6-membered benzyl group for 5-membered heterocycles (38 and 39) resulted in compounds that were inactive, indicating that the benzyl group is essential for activity. Incorporation of a branched methyl in the benzyl position (37) reduced the activity of the compound, suggesting that there may be a steric clash at the binding site.

A

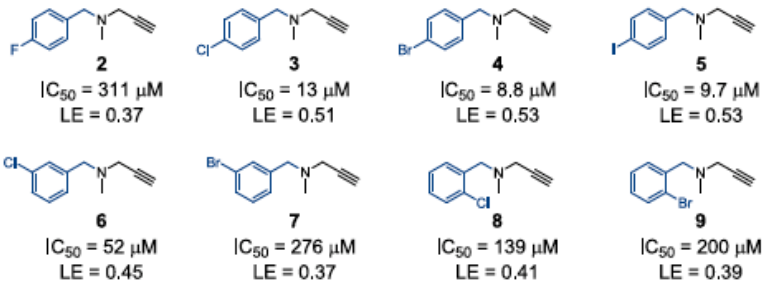

2
IC_{50} = 311 µM
LE = 0.37

3
IC_{50} = 13 µM
LE = 0.51

4
IC_{50} = 8.8 µM
LE = 0.53

5
IC_{50} = 9.7 µM
LE = 0.53

6
IC_{50} = 52 µM
LE = 0.45

7
IC_{50} = 276 µM
LE = 0.37

8
IC_{50} = 139 µM
LE = 0.41

9
IC_{50} = 200 µM
LE = 0.39

B

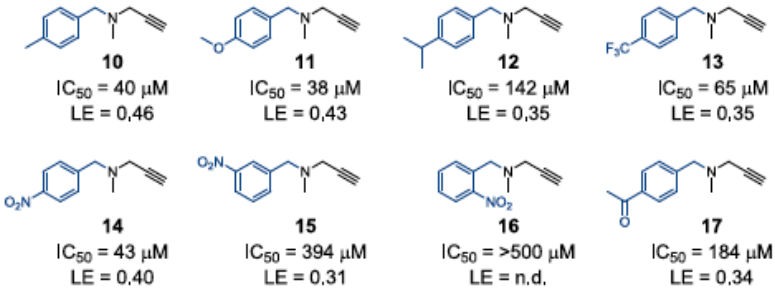

10
IC_{50} = 40 µM
LE = 0,46

11
IC_{50} = 38 µM
LE = 0,43

12
IC_{50} = 142 µM
LE = 0,35

13
IC_{50} = 65 µM
LE = 0,35

14
IC_{50} = 43 µM
LE = 0,40

15
IC_{50} = 394 µM
LE = 0,31

16
IC_{50} = >500 µM
LE = n.d.

17
IC_{50} = 184 µM
LE = 0,34

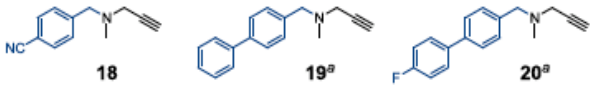

18
IC_{50} = >500 µM
LE = n,d,

19[a]
IC_{50} = 315 µM
LE = 0,27

20[a]
IC_{50} = 211 µM
LE = 0,26

C

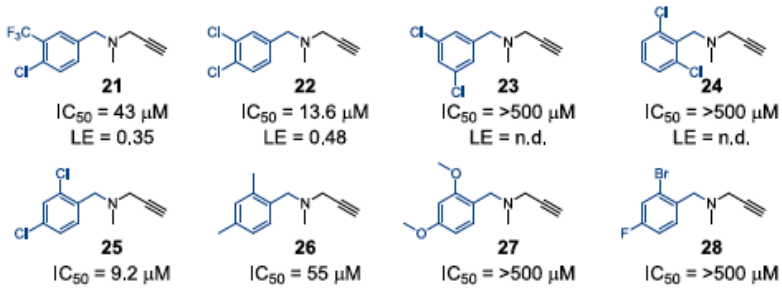

21
IC_{50} = 43 µM
LE = 0,35

22
IC_{50} = 13.6 µM
LE = 0,48

23
IC_{50} = >500 µM
LE = n.d.

24
IC_{50} = >500 µM
LE = n.d.

25
IC_{50} = 9.2 µM
LE = 0,49

26
IC_{50} = 55 µM
LE = 0,42

27
IC_{50} = >500 µM
LE = n,d,

28
IC_{50} = >500 µM
LE = n,d,

29
IC_{50} = 66 µM
LE = 0.41

30
IC_{50} = 42 µM
LE = 0.43

31
IC_{50} = 34 µM
LE = 0.44

32
IC_{50} = 228 µM
LE = 0.36

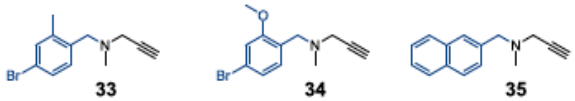

33
IC_{50} = 38 µM
LE = 0.43

34
IC_{50} = 21 µM
LE = 0.43

35
IC_{50} = 21 µM
LE = 0.28

D

36
IC_{50} = >500 µM
LE = n.d.

37
IC_{50} = 316 µM
LE = 0.34

38
IC_{50} = >500 µM
LE = n.d.

39
IC_{50} = >500 µM
LE = n.d.

Fig. 2. A: SAR of halogen substitutions (blue). B: SAR of non-halogen substitutions (blue). C: SAR of disubstitutions (blue). D: SAR of non-benzyl substitutions (blue). [a] Prepared by Suzuki-Miyaura cross-coupling.

With the 4-bromobenzyl moiety identified as the optimal group for PYCR1 inhibition, and this motif was carried on throughout the rest of the SAR exploration.

The second group assessed was the N-methyl moiety as outlined in Fig. 3. There was markedly less tolerance in this group than with the benzyl group with only four analogues showing any measurable activity against the enzyme. Carbon chains longer than an ethyl group (42 and 43) were found to be inactive as were branched moieties (44 and 45). Indeed, of the alkyl substituents only ethyl (41) was active, albeit less so than the methyl substituent of compound 4. Having no substituent on the nitrogen core (40) also resulted in a less potent compound. Larger groups such as 4-bromo benzyl (47) and isoxazolyl (46) were moderately active. However, the higher molecular weight of these compounds, resulted in a lower LE. Larger substituents such as 48 were found not to be tolerated. Tethering the N-group to the benzyl group was also not tolerated with the isoindoline and tetrahydroisoquinoline (49 and 50, respectively) both being inactive. This could be due to the molecules being constrained in the wrong conformation for binding to the target. The final changes assessed were to the nature of the nitrogen core, with the introduction of an amide (51) or sulfonamide (52) in the place of a basic tertiary amine. Both of these were inactive suggesting that a basic amine is necessary for activity.

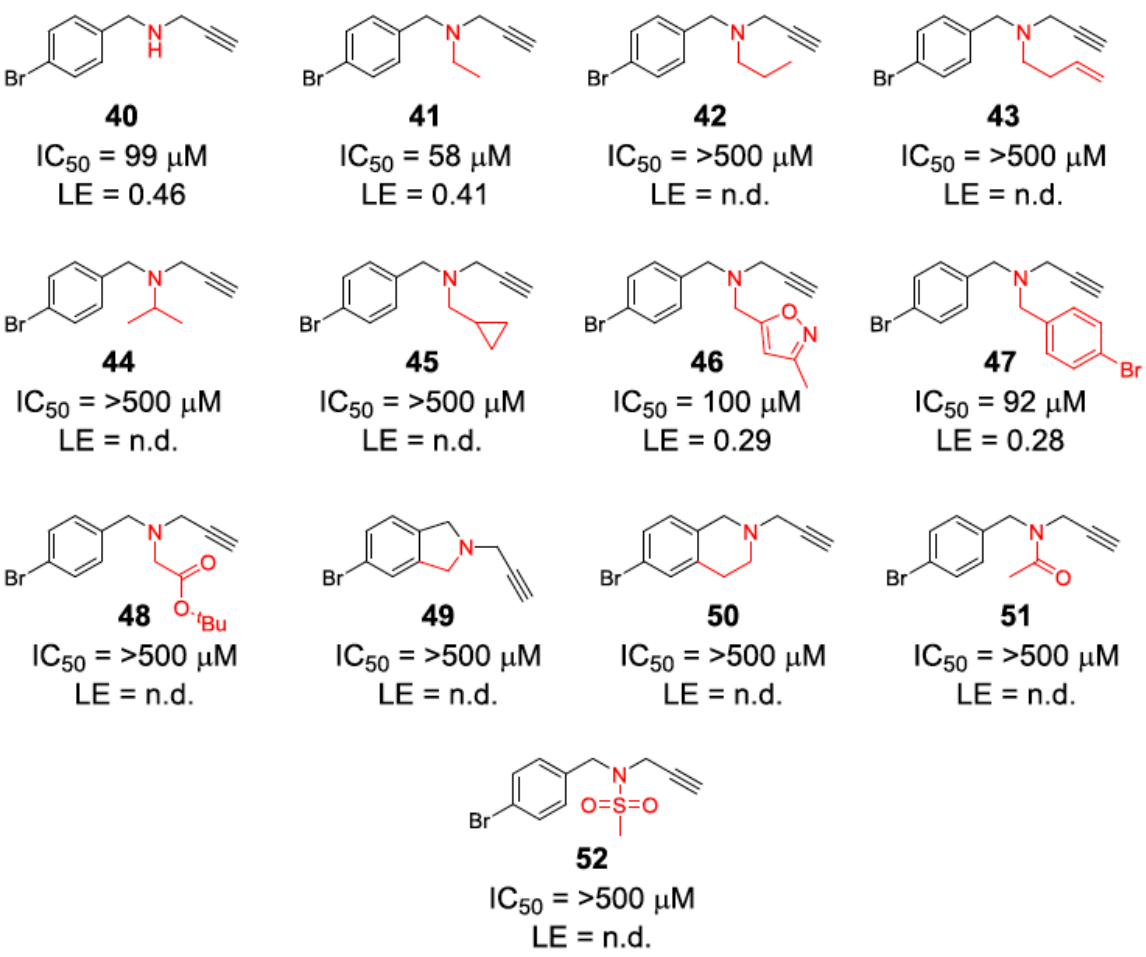

Fig. 3. Structure and activity of alterations to the N-methyl group (red).

The last modifications examined were alterations to the propargyl moiety, as outlined in Fig. 4. As with the N-methyl group, there was limited tolerance in changes to this group. Fully reducing (55) or completely removing the propargyl group (53) resulted in inactive derivatives, while reduction to the propenyl analogue (54) drastically reduced activity. Introduction of a benzyl (57) and cyclopropyl group (58) also resulted in inactive compounds and suggests the alkyne component of the molecule is required. Homologation (56) and incorporation of a branched methyl to the propargyl unit (61) resulted in a considerable reduction in potency. In the case of the branched analogue, this could be due to a steric restriction in the binding site, however, further cements the need for a propargyl amine for optimum potency. Finally, the terminal alkyne was exchanged for internal alkynes 59 and 60. Pleasingly, these compounds retained some degree of potency which decreased when the size of the capping group increased. However, they remained less potent than compound 4, which again could be attributed to a steric

constraint. It should be noted that further structural data would be required to corroborate this hypothesis.

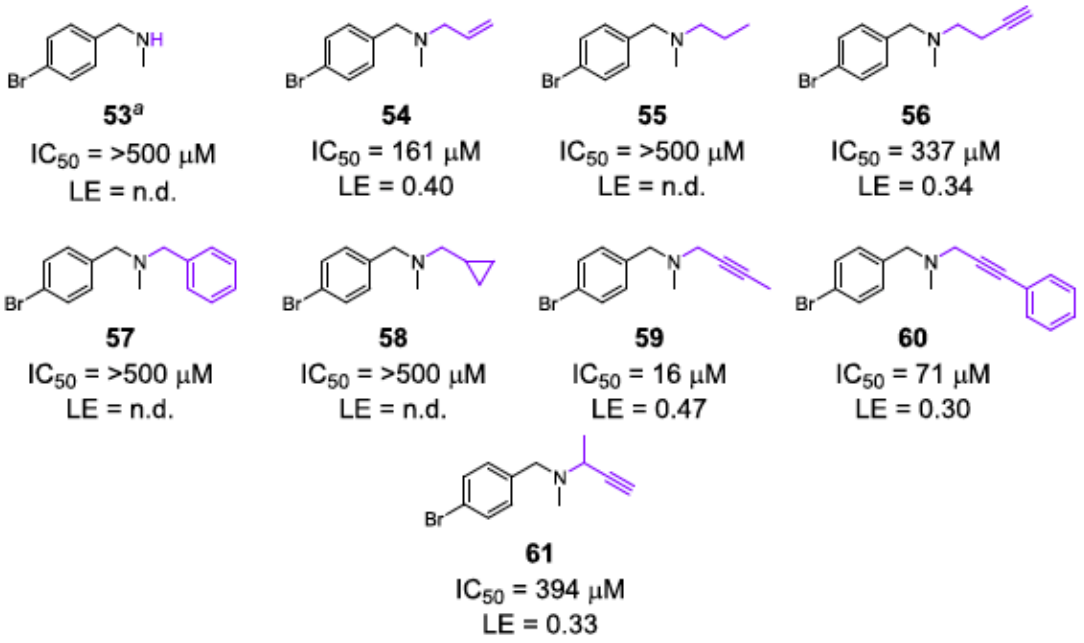

Fig. 4. Structure and activity of changes to the propargyl group (purple). [a]Commercially available feedstock.

Compound 4 was found to be the most active of all the analogues synthesized and accordingly was advanced for further biological evaluation as the lead compound.

The first study considered was measurement of endogenous proline levels by LC-MS. As the inhibition of PYCR1 should prevent the formation of proline, compound 4 should lower the concentration of intracellular proline. Thus, a human breast cancer cell line (SUM159-PT) was incubated with compound 4 at serial concentrations of 1, 5, 20 and 100 µM, respectively, with pargyline (100 µM) as a positive control. As outlined in Fig. 5a, pargyline supplementation at a concentration of 100 µM could reduce endogenous proline level by approximately 50% compared to mock treatment. Intriguingly, compound 4 even at 5 µM could already strongly reduce proline levels despite the inhibition was somehow impaired at higher concentration of 100 µM. The increase in proline levels might be attributed to the limited solubility of compound 4 in the buffer at higher concentrations. Notably, almost no effect on the levels of other amino acids was detected with either pargyline or compound 4 (Fig. S1, Supplementary Material). In order to show if the reduction of proline was due to PYCR1 inhibition, we performed a ^{13}C-glutamine tracing experiment. By culturing cells with [U-^{13}C]-glutamine, we followed the

incorporation of ^{13}C from glutamine, via glutamate, in proline (M+5), as shown in Fig. 5b. After 24 h incubation with compound 4, proline derived from labeled glutamine (M+5) is less presented compared to mock treatment. These data further confirmed that compound 4 could inhibit PYCR1 activity and thus lead to lower endogenous proline level.

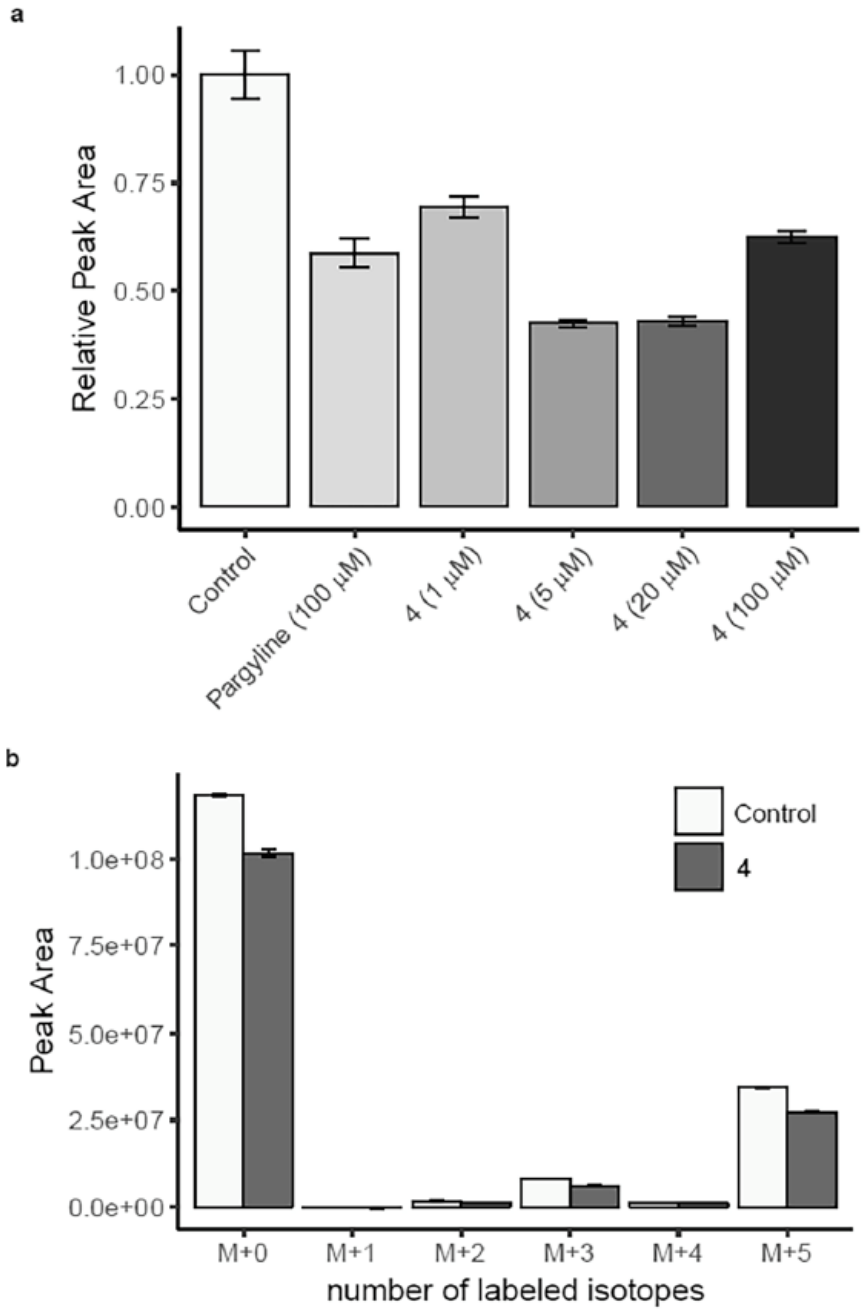

Fig. 5. (a) Results of the LC–MS based amino acid assay, showing the quantity of proline present in lysed human breast cancer cells (SUM159-PT) after incubation with pargyline and compound 4. (b) Results of the glutamine flux study showing lower levels of proline (M+5) after incubation with compound 4 (5 µM).

All the above data indicates that both pargyline and compound 4 could inhibit PYCR1, thus causing a measurable, pathway relevant, biological response. To the best of our knowledge, this represents the first time such a phenotypic response has been observed using small molecules as PYCR1 inhibitors.

To examine the effectivity of compound 4 under cell culture conditions, two breast cancer cell lines, MDA-MB-231 and SUM159-PT, were separately incubated with or without compound 4. Both cell lines have relatively high PYCR1 levels, and depend on PYCR1 activity for proliferation and tumor formation (Loayza-Puch *et al*, 2016). Interestingly, following the incubation of compound 4 (10 μM), cell proliferation of both MDA-MB-231 and SUM159-PT was impaired (data not shown). As expected, the supplementation of proline to the medium rescued the adverse effect of compound 4.

In conclusion, over 60 potential small molecule inhibitors of PYCR1 were synthesized in order to probe the SAR around PYCR1 inhibition. Of all the synthesized analogues, compound 4 (termed Proline Production Inhibitor-1, ProPI-1) was identified as the most potent in the PYCR1 inhibition assay with an IC_{50} of 8.8 μM, approximately 20 times more potent than that of pargyline, with the most efficient binding as evidenced by a LE of 0.53. As a result of this, ProPI-1 was taken forward as a lead into a series of pathway relevant biological tests and, was found to significantly reduce endogenous proline level and inhibit cancer cell proliferation. Further work is to obtain an X-ray crystal structure of ProPI-1 and PYCR1, as well as validation of the efficacy of PYCR1 inhibitor, ProPI *in vivo*.

Supplementary data (Experimental procedures and characterization data of all pargyline analogues and protocol for PYCR1 testing) to this article can be found online at https://doi.org/10.1016/j.bmcl.2019.07.047.

References

Cai F, Miao Y, Liu C, Wu T, Shen S, Su X & Shi Y (2018) Pyrroline-5-carboxylate reductase 1 promotes proliferation and inhibits apoptosis in non-small cell lung cancer. *Oncol. Lett.*

Chen H, Engkvist O & Kogej T (2015) Compound Properties and Their Influence on Drug Quality. In *The Practice of Medicinal Chemistry: Fourth Edition*

Christensen EM, Patel SM, Korasick DA, Campbell AC, Krause KL, Becker DF & Tanner JJ

(2017a) Resolving the cofactor-binding site in the proline biosynthetic enzyme human pyrroline-5-carboxylate reductase 1. *J. Biol. Chem.*

Christensen EM, Patel SM, Korasick DA, Campbell AC, Krause KL, Becker DF & Tanner JJ (2017b) Resolving the cofactor-binding site in the proline biosynthetic enzyme human pyrroline-5-carboxylate reductase 1. *J. Biol. Chem.* **292:** 7233–7243

Craze ML, Cheung H, Jewa N, Coimbra NDM, Soria D, El-Ansari R, Aleskandarany MA, Wai Cheng K, Diez-Rodriguez M, Nolan CC, Ellis IO, Rakha EA & Green AR (2018) MYC regulation of glutamine-proline regulatory axis is key in luminal B breast cancer. *Br. J. Cancer* **118:** 258–265

Ding J, Kuo ML, Su L, Xue L, Luh F, Zhang H, Wang J, Lin TG, Zhang K, Chu P, Zheng S, Liu X & Yen Y (2017) Human mitochondrial pyrroline-5-carboxylate reductase 1 promotes invasiveness and impacts survival in breast cancers. *Carcinogenesis*

Ford MC & Ho PS (2016) Computational Tools to Model Halogen Bonds in Medicinal Chemistry. *J. Med. Chem.*

de Ingeniis J, Ratnikov B, Richardson AD, Scott DA, Aza-Blanc P, De SK, Kazanov M, Pellecchia M, Ronai Z, Osterman AL & Smith JW (2012) Functional Specialization in Proline Biosynthesis of Melanoma. *PLoS One*

Kang X, He W, Huang Y, Yu Q, Chen Y, Gao X, Sun X & Fan Y (2016) Introducing precise genetic modifications into human 3PN embryos by CRISPR/Cas-mediated genome editing. *J. Assist. Reprod. Genet.*

Kim JH, Nam B, Choi YJ, Kim SY, Lee JE, Sung KJ, Kim WS, Choi CM, Chang EJ, Koh JS, Song JS, Yoon S, Lee JC, Rho JK & Son J (2018) Enhanced glycolysis supports cell survival in EGFR-Mutant lung adenocarcinoma by inhibiting autophagy-mediated EGFR degradation. *Cancer Res.*

Lane AN & Fan TWM (2015) Regulation of mammalian nucleotide metabolism and biosynthesis. *Nucleic Acids Res.*

Liang P, Xu Y, Zhang X, Ding C, Huang R, Zhang Z, Lv J, Xie X, Chen Y, Li Y, Sun Y, Bai Y, Songyang Z, Ma W, Zhou C & Huang J (2015) CRISPR/Cas9-mediated gene editing in human tripronuclear zygotes. *Protein Cell*

Liang X, Zhang L, Natarajan SK & Becker DF (2013) Proline mechanisms of stress survival. *Antioxidants Redox Signal.*

Loayza-Puch F, Rooijers K, Buil LCM, Zijlstra J, F. Oude Vrielink J, Lopes R, Ugalde AP, van Breugel P, Hofland I, Wesseling J, van Tellingen O, Bex A & Agami R (2016) Tumour-specific proline vulnerability uncovered by differential ribosome codon reading. *Nature* **530:**

490–494 Available at: http://dx.doi.org/10.1038/nature16982

Petropoulos S, Edsgärd D, Reinius B, Deng Q, Panula SP, Codeluppi S, Plaza Reyes A, Linnarsson S, Sandberg R & Lanner F (2016) Single-Cell RNA-Seq Reveals Lineage and X Chromosome Dynamics in Human Preimplantation Embryos. *Cell*

Phang JM, Donald SP, Pandhare J & Liu Y (2008) The metabolism of proline, a stress substrate, modulates carcinogenic pathways. *Amino Acids*

Selkirk SM (2004) Gene therapy in clinical medicine. *Postgrad. Med. J.*

Song S, Jacobson KN, McDermott KM, Reddy SP, Cress AE, Tang H, Dudek SM, Black SM, Garcia JGN, Makino A & Yuan JXJ (2016) ATP promotes cell survival via regulation of cytosolic [Ca2+] and Bcl-2/Bax ratio in lung cancer cells. *Am. J. Physiol. - Cell Physiol.*

Stepan AF, Subramanyam C, Efremov I V., Dutra JK, O'Sullivan TJ, Dirico KJ, McDonald WS, Won A, Dorff PH, Nolan CE, Becker SL, Pustilnik LR, Riddell DR, Kauffman GW, Kormos BL, Zhang L, Lu Y, Capetta SH, Green ME, Karki K, et al (2012) Application of the bicyclo[1.1.1]pentane motif as a nonclassical phenyl ring bioisostere in the design of a potent and orally active γ-secretase inhibitor. *J. Med. Chem.* **55:** 3414–3424

Tanner JJ, Fendt SM & Becker DF (2018) The Proline Cycle As a Potential Cancer Therapy Target. *Biochemistry*

Zeng T, Zhu L, Liao M, Zhuo W, Yang S, Wu W & Wang D (2017) Knockdown of PYCR1 inhibits cell proliferation and colony formation via cell cycle arrest and apoptosis in prostate cancer. *Med. Oncol.*

Chapter 5
General Discussion

The potential of L-asparaginase in treating solid tumors still needs to be further explored

L-asparaginase (ASNase) has achieved great success in treating childhood acute lymphoblastic leukemia (ALL)[1]. Till now, it is the only FDA approved drug for amino acid deprivation in clinic. Notably, ASNase has a dual asparagine and glutamine deaminase activity even though the glutaminase activity was not required for its anticancer effect with ASNS-negative cancer cells[2]. We observed that in cell culture conditions, both asparagine and glutamine were robustly depleted by ASNase while *in vivo* conditions, the efficacy to deplete glutamine was far less effective compared to that of asparagine[3]. And the potent capability to deplete asparagine in tissues and expanding tumors by ASNase was absolutely impressive[3], which leaves space to explore cancer vulnerability under asparagine depletion conditions by ASNase.

ASNS is essential but not sufficient for ASNase resistance

Asparagine synthetase (ASNS) was the gene responsible for the endogenous asparagine synthesis. Accordingly, under asparagine depletion by ASNase, ASNS expression was taken for granted to be the reason for ASNase resistance[4]. However, this was somehow controversial: first of all, researchers found that ASNase was still effective with ALL even though ASNS was expressed[5,6]; secondly, the upregulated ASNS could not synthesize enough asparagine to compensate for the depletion by ASNase[3]. Protein degradation for asparagine supply has been proposed to contribute to ASNase resistance in ALL, again, whether this could produce enough asparagine to rescue the severe asparagine depletion by ASNase treatment, and whether the newly “produced” asparagine was still available in the presence of ASNase (probably immediately degraded) needs to be further investigated[7]. Despite some reported the effectivity of ASNase in ASNS-negative solid tumors, we proposed that the activation of general amino acid sensing axis GCN2-ATF4-ASNS was an essential response to ASNase treatment, or other amino acid starvation or nutrient depletion, which was not sufficient to reduce the resistance[3,8–10].

SLC1A3 mediated aspartate/glutamate uptake contributed to ASNase resistance

By performing a genome-wide drop-out screen, we found the loss of function of SLC1A3, a cytoplasmic transporter for aspartate/glutamate, could sensitize cancer cells to ASNase resistance[3]. This was interesting and reasonable as aspartate and glutamate were exactly the

substrates for endogenous synthesis of asparagine and glutamine, which could be degraded by ASNase. Besides, we observed that following ASNase treatment, PC3 cells presented increased consumption of aspartate and glutamate to maintain cell proliferation. SLC1A3 blockage in combination with ASNase treatment caused either cell cycle arrest or apoptosis in cancer cells which were originally resistant to ASNase. Meanwhile, we also observed compromised function of TCA cycle, urea cycle, nucleotide synthesis, energy production, redox homeostasis and lipid biosynthesis. Notably, the specific expression pattern of SLC1A3 in brain tissue under normal conditions might supply a specific target for tumors. Recently, the role of aspartate has gained so much attention that the involvement of glutamate in cancer progression was largely ignored[11–14]. This was biased as: (1), aspartate and glutamate could be converted mutually; and (2), the transportation of aspartate was usually coupled with exchange with glutamate. Overall, our findings were in consistency with a previous study, where aspartate metabolism was predicted for ASNase resistance in primary ALL samples[15].

Overall, CRISPR screens serve as an efficient platform to target cancer vulnerability, which might help to improve drug performance or identification of new drugs for cancer therapeutic purpose in clinic. Restricting onco-amino acids or other nutrients by interference either with corresponding transportation or endogenous synthesis, or even in combination if necessary, might provide a potential strategy for cancer treatment.

References

1 Pui C-H, Campana D, Pei D, Bowman WP, Sandlund JT, Kaste SC *et al.* Treating Childhood Acute Lymphoblastic Leukemia without Cranial Irradiation. *N Engl J Med* 2009; **360**: 2730–2741.

2 Chan WK, Lorenzi PL, Anishkin A, Purwaha P, Rogers DM, Sukharev S *et al.* The glutaminase activity of L-asparaginase is not required for anticancer activity against ASNS-negative cells. *Blood* 2014; **123**: 3596–3606.

3 Sun J, Nagel R, Zaal EA, Ugalde AP, Han R, Proost N *et al.* SLC1A3 contributes to L-asparaginase resistance in solid tumors. *EMBO J* 2019; **38**. doi:10.15252/embj.2019102147.

4 Scherf U, Ross DT, Waltham M, Smith LH, Lee JK, Tanabe L *et al.* A gene expression database for the molecular pharmacology of cancer. *Nat Genet* 2000; **24**: 236–244.

5 Stams WAG. Sensitivity to L-asparaginase is not associated with expression levels of asparagine synthetase in t(12;21)+ pediatric ALL. *Blood* 2003; **101**: 2743–2747.

6 Vander Heiden MG, DeBerardinis RJ. Understanding the Intersections between Metabolism and Cancer Biology. *Cell* 2017; **168**: 657–669.

7 Hinze L, Pfirrmann M, Karim S, Degar J, McGuckin C, Vinjamur D *et al.* Synthetic lethality of Wnt pathway activation and asparaginase in drug-resistant acute leukemias. *Cancer Cell* 2019; **35**: 664-676.e7.

8 Ye J, Kumanova M, Hart LS, Sloane K, Zhang H, De Panis DN *et al.* The GCN2-ATF4 pathway is critical for tumour cell survival and proliferation in response to nutrient deprivation. *EMBO J* 2010; **29**: 2082–2096.

9 Nakamura A, Nambu T, Ebara S, Hasegawa Y, Toyoshima K, Tsuchiya Y *et al.* Inhibition of GCN2 sensitizes ASNS-low cancer cells to asparaginase by disrupting the amino acid response. *Proc Natl Acad Sci* 2018; **115**: E7776–E7785.

10 Li H, Ning S, Ghandi M, Kryukov G V., Gopal S, Deik A *et al.* The landscape of cancer cell line metabolism. *Nat Med* 2019; **25**: 850–860.

11 Alkan HF, Walter KE, Luengo A, Madreiter-Sokolowski CT, Stryeck S, Lau AN *et al.* Cytosolic Aspartate Availability Determines Cell Survival When Glutamine Is Limiting. *Cell Metab* 2018; **28**: 706-720.e6.

12 Garcia-Bermudez J, Baudrier L, La K, Zhu XG, Fidelin J, Sviderskiy VO *et al.* Aspartate is a limiting metabolite for cancer cell proliferation under hypoxia and in tumours. *Nat Cell Biol* 2018; **20**: 775–781.

13 Sullivan LB, Luengo A, Danai L V., Bush LN, Diehl FF, Hosios AM *et al.* Aspartate is an endogenous metabolic limitation for tumour growth. *Nat Cell Biol* 2018; **20**: 782–788.

14 Tajan M, Hock AK, Blagih J, Robertson NA, Labuschagne CF, Kruiswijk F *et al.* A Role for p53 in the Adaptation to Glutamine Starvation through the Expression of SLC1A3. *Cell Metab* 2018; **28**: 721-736.e6.

15 Chen S-H, Yang W, Fan Y, Stocco G, Crews KR, Yang JJ *et al.* A genome-wide approach identifies that the aspartate metabolism pathway contributes to asparaginase sensitivity. *Leukemia* 2011; **25**: 66–74.

Summary

Early in 1961, L-asparaginase (ASNase), originated from guinea pig serum, was found to have anti-lymphoma effect and later on it was approved by the Food and Drug Administration (FDA), and incorporated for acute lymphoblastic leukemia treatment. So far, the progress of ASNase in childhood ALL is quite impressive, with an overall survival rate of ~90%. This had greatly encouraged further application of ASNase in other tumor types. However, several clinical trials indicated severe toxicity of ASNase due to increasing dosage. Asparagine synthetase (ASNS) was canonically proposed to be responsible for ASNase resistance. However, we thought the general nutrient sensing machinery (GCN2-ATF4-ASNS axis) as a common and essential response to nutrient starvation but not sufficient to induce this resistance. Hence, it was of great interests to investigate if other genes or pathways were involved in ASNase response besides the GCN2-ATF4-ASNS axis.

In this thesis, we initiated a genome-wide CRISPR functional screen in PC3 cells and identified SLC1A3 as a contributor to ASNase resistance. SLC1A3 was normally and restrictedly expressed in brain tissues. Interestingly, high SLC1A3 expression was also observed in some tumor types. This specific expression pattern might benefit drug target effectivity.

Notably, except for amino acid, lipid-related metabolites could also be imported by corresponding transporters, indicating investigation on transporter(s) mediated nutrient convey might be urgent for our understanding of cancer metabolism and malignancy. And the pathways of endogenous synthesis of onco-amino acids or other nutrients that support cancer progression could also be critical targets for therapeutic purpose.

Besides, we also explored the development of inhibitors targeting proline endogenous synthesis and examined their effects on cancer cell proliferation.

In summary, restricting the availability of onco-amino acids might impair cancer cell malignancy and thus provide further clues for clinical research.

Samenvatting

Begin 1961 bleek L-asparaginase (ASNase), afkomstig van cavia-serum, een anti-lymfoomeffect te hebben en later werd het goedgekeurd door de Food and Drug Administration (FDA) en opgenomen voor acute lymfoblastaire leukemiebehandeling. Tot nu toe is de voortgang van ASNase in ALL bij kinderen behoorlijk indrukwekkend, met een algemeen overlevingspercentage van ~ 90%. Dit had de verdere toepassing van ASNase in andere tumortypen enorm gestimuleerd. Verschillende klinische onderzoeken wezen echter op ernstige toxiciteit van ASNase als gevolg van de toenemende dosering. Asparagine synthetase (ASNS) is volgens de canoniek verantwoordelijk voor ASNase resistentie. We dachten echter dat de algemene machines voor het meten van voedingsstoffen (GCN2-ATF4-ASNS-as) een veelvoorkomende en essentiële reactie waren op uithongering van voedingsstoffen, maar niet voldoende om deze weerstand te induceren. Daarom was het van groot belang om te onderzoeken of naast de GCN2-ATF4-ASNS-as andere genen of paden betrokken waren bij ASNase-respons.

In dit proefschrift hebben we een genoom breed CRISPR-functioneel scherm in PC3-cellen geïnitieerd en SLC1A3 geïdentificeerd als een bijdrage aan ASNase-resistentie. SLC1A3 werd normaal en beperkt tot expressie gebracht in hersenweefsels. Interessant is dat bij sommige tumortypen ook hoge SLC1A3-expressie werd waargenomen. Dit specifieke expressiepatroon kan de doelgerichtheid van het geneesmiddel ten goede komen.

Met name, met uitzondering van aminozuur, kunnen lipide-gerelateerde metabolieten ook worden geïmporteerd door overeenkomstige transporters, wat aangeeft dat onderzoek naar door transporter(s) gemedieerde nutriëntentransport mogelijk dringend is voor ons begrip van het metabolisme van kanker en maligniteit. En de routes van endogene synthese van onco-aminozuren of andere voedingsstoffen die de progressie van kanker ondersteunen, kunnen ook kritische doelen zijn voor therapeutische doeleinden.

Daarnaast hebben we ook de ontwikkeling van remmers gericht op endogene proline-synthese onderzocht en hun effecten op de proliferatie van kankercellen onderzocht.

Samenvattend kan het beperken van de beschikbaarheid van onco-aminozuren de maligniteit van kankercellen verminderen en zo verdere aanwijzingen geven voor klinisch onderzoek.

List of publications

Sun J, Nagel R, Zaal EA, Ugalde AP, Han R, Proost N *et al.* SLC1A3 contributes to L-asparaginase resistance in solid tumors. *EMBO J* doi:10.15252/embj.2019102147.

Milne K, **Sun J**, Zaal EA, Mowat J, Celie PHN, Fish A *et al.* A fragment-like approach to PYCR1 inhibition. *Bioorg Med Chem Lett* 2019. doi:10.1016/j.bmcl.2019.07.047.

Sun J & Agami R Aberrant onco-amino acid acquisition in cancer cells (review)

Sun J, Huang L, Wei Y, Wang Y, Chen D, Du W *et al.* Identification of three PPV1 VP2 protein-specific B cell linear epitopes using monoclonal antibodies against baculovirus-expressed recombinant VP2 protein. *Appl Microbiol Biotechnol* 2015; **99**: 9025–9036.

Sun J, Huang L, Wei Y, Wang Y, Chen D, Du W *et al.* Prevalence of emerging porcine parvoviruses and their co-infections with porcine circovirus type 2 in China. *Arch Virol* 2015; **160**: 1339–1344.